January 2016

Optical Emission Spectroscopy of High Voltage Cold Atmospheric Plasma Generated Using Dielectric Barrier Discharges

Russell Scott Brayfield II
Purdue University

PURDUE UNIVERSITY
GRADUATE SCHOOL
Thesis/Dissertation Acceptance

This is to certify that the thesis/dissertation prepared

By Russell S. Brayfield II

Entitled
Optical Emission Spectroscopy of High Voltage Cold Atmospheric Plasma Generated Using Dielectric Barrier Discharges

For the degree of Master of Science in Nuclear Engineering

Is approved by the final examining committee:

Allen L. Garner
Chair

Gennady Miloshevsky

Kevin M. Keener

To the best of my knowledge and as understood by the student in the Thesis/Dissertation Agreement, Publication Delay, and Certification Disclaimer (Graduate School Form 32), this thesis/dissertation adheres to the provisions of Purdue University's "Policy of Integrity in Research" and the use of copyright material.

Approved by Major Professor(s): Allen L. Garner

Approved by: Takashi Hibiki 11/18/2016

Head of the Departmental Graduate Program Date

OPTICAL EMISSION SPECTROSCOPY OF HIGH VOLTAGE COLD ATMOSPHERIC PLASMA GENERATED USING DIELECTRIC BARRIER DISCHARGES

A Thesis

Submitted to the Faculty

of

Purdue University

by

Russell S. Brayfield II

In Partial Fulfillment of the

Requirements for the Degree

of

Master of Science in Nuclear Engineering

December 2016

Purdue University

West Lafayette, Indiana

For my parents, who have always supported me in everything I do and taught me to question everything. You instilled the moral values and work ethic that has led me to where I am today.

For my grandmother and grandfather, who has always encouraged me to go after my dreams and supported me along the way in life no matter what I may have needed.

For Dr. Allen Garner, who gave me the opportunity to explore my passions and guided my growth as a researcher. Your mentorship has expanded my understanding of engineering and led me to better understand what I want out of life.

For my wife, Rebecca, who has had faith in me even when I lost mine. You have been my emotional anchor through the long nights and stress. Without your support I could not have made it through to where I am now.

ACKNOWLEDGEMENTS

Many people have contributed to my worked presented here and each has left a lasting impression on my life. First, I would like to acknowledge Dr. Prasoon Diwakar, who not only helped me understand the fundamentals of diagnostics but also taught me how to approach plasma research. You took time out of your extremely busy schedule to meet with me whenever I needed to discuss research or problems with experiments. Second, I would like to thank Nick and Andrew, who have helped me in countless ways both in research and life and made the long nights working enjoyable. Nick has proofread almost everything I've written working towards this degree, so I am sure he is glad to see it come to an end. Andrew has been the springboard for countless ideas and discussions over the years, both about research and life. He has been a reliable friend to call on when help was needed and for that cannot be thanked enough. Third, I would like to thank Dr. Robert Bean, who guided me through the frustrations of graduate school and research and has become a close friend. He has been a guide through the murky waters of graduate life and work and has helped develop professional and research skills that have proved invaluable. I would also like to thank Toni, Tiffany, and Kellie, without their help behind the scenes administrative tasks would be daunting. They are truly the back bone of our department. Next I would like to thank my advisor Dr. Allen Garner, who has guided me

in every way possible in graduate school and helped me grow beyond what I thought possible. His guidance and support has not only helped me grow as a researcher but also personally and professionally and has helped set the tone for my career. Lastly I would like to thank my wife Rebecca, for everything she has done over the years to support me in my education and in life. She has supported me emotionally, financially and spiritually every step of the way. She has been by my side every step of the way and I truly could not have done this without her.

TABLE OF CONTENTS

APPENDICES

LIST OF TABLES

LIST OF FIGURES

Figure Page

Figure Page

Figure Page

NOMENCLATURE

CAP – Cold Atmospheric Plasma

HVCAP – High Voltage Cold Atmospheric Plasma

OES – Optical Emission Spectroscopy

OAS – Optical Absorption Spectroscopy

DBD – Dielectric Barrier Discharge

RF – Radio Frequency

LTE – Local Thermal Equilibrium

PLTE – Partial Local Thermal Equilibrium

CCD – Charge Coupled Device

ICCD – Intensified Charge Coupled Device

ABSTRACT

Brayfield, Russell, S. M.S.N.E., Purdue University, December 2016. Optical Emission Spectroscopy of High Voltage Cold Atmospheric Plasma Generated Using Dielectric Barrier Discharges. Major Professor: Allen Garner.

While numerous experiments have demonstrated the efficacy of high voltage cold atmospheric pressure plasmas for extending food shelf-life and sterilizing medical instrumentation in sealed packages, the influence of the packaging material and gas composition on the reactive gas species generated by the high voltage atmospheric cold plasma is poorly understood. This study elucidates the impact of these parameters on plasma generation in sealed packages for four gases (ambient air, commercial grade compressed air, and high purity helium and nitrogen) placed in commercially available transparent plastic containers and bags. After adequate gas flushing, we observed that the container and bag individually reduced signal intensity by 63% and 45% across the measured wavelengths of 200 nm to 1100 nm, demonstrating that they acted as broadband absorbers. Neither the container nor bag influenced the wavelengths of the peak emissions, only the amplitude, indicating no significant effect on the types of species generated. Lissajous diagrams showed that the power dissipated by the nitrogen and ambient air plasma generated at 72 ± 3.7 kV RMS were comparable to the compressed dry air discharge generated at 80 ± 3.7 kV RMS.

The helium discharge at 37 ± 3.7 kV RMS absorbed approximately 92% more power than these gases. We observed translational temperatures ranging from 1088 K for nitrogen to 1421 K for compressed air and rotational temperatures ranging from 285 K for helium to 479 K for compressed air. These results indicate that packaging materials have minimal effect on the most dominant peaks although further studies are required to elucidate the impact on less intense peaks observed.

We next assessed the effect of voltage on species generation using a helium air plasma generated using the Phenix system with applied voltages of 36.4, 44.8, 58.1, and 71.0 kV. The light from the plasma was collected using a fiber optic cable that was provided with the SP2500 spectrometer. The N_2 Second Positive system of a helium air plasma generated at 36.4 kV was observed using the 1800 g/mm grating of a spectrometer. SPECAIR fits for the spectra show no real correlation to voltage. Higher voltage did not necessarily translate to higher plasma temperature although the relative intensities for the observed peaks increased with increasing voltage. This clearly showed that the increased voltage did not directly correlate to increased temperature of the bulk gas.

CHAPTER 1. INTRODUCTION

Plasmas generated at or near atmospheric pressure are typically thermal plasmas with temperatures well above room temperature. For instance, a typical glow discharge used to deposit carbon films had a temperature between 300 K and 400 K [1]. The first ionization potential of helium, another common gas used for atmospheric pressure plasmas, is approximately 12000 K, which is well above room temperature [2]. These high plasma temperatures lead to thermal transfer between the plasma and any surrounding medium, which has been leveraged in many applications that call for high heat applications. For instance, steel processing facilities routinely use arc plasma heaters to melt raw metal for processing [3]. These heaters are placed in large crucibles to melt large quantities of metal for various foundry uses. Another industrial application has led to plasma cutters becoming commonplace in many shops today [3–5]. Thermal plasma has also been applied to creating thin diamond films with radio frequency (RF) generated discharges [6]. Ten minute applications of RF (4 MHz, 60 kW) argon, hydrogen, and methane plasmas formed 10-30 μm crystals with a deposition rate of 1 $\mu m/min$.

While cold atmospheric plasmas (CAPs) have historically been used in industries for etching, deposition, cleaning, and flat panel displays [7,8],recent studies have evaluated for biological applications [9].

CAPs are non-equilibrium plasmas formed at or near room temperature. In plasma near room temperature, the high energy electrons do not collide as often with the low energy ions (gas particles); therefore, the electrons and various ions are not in thermodynamic equilibrium. Non-equilibrium plasmas are generated when the pressure is sufficiently low such that particle collisions in the gas are less frequent than at higher pressures [2]. Because relatively few collisions occur at low pressure, the bulk of the plasma and gas remain near room temperature [2]. To achieve this at atmospheric pressure, radio frequency (RF) or pulsed power systems generate high frequency electromagnetic fields to "pump" the electrons and create the discharge [2]. Generating CAP discharges requires minimizing operating voltage, discharge current, and the duty cycle of the "pumping" pulses [10].

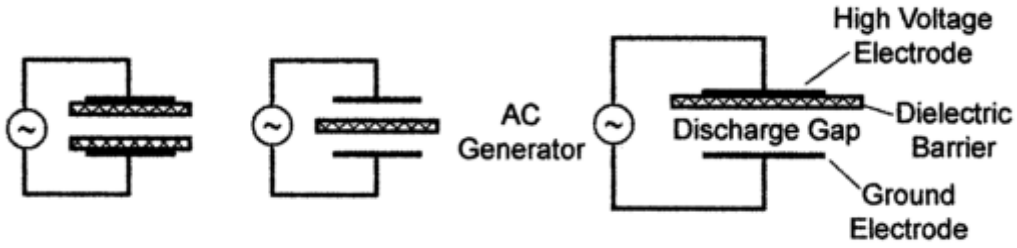

Figure 1: Sample DBD configurations from [11].

The most common method for CAP generation is the silent discharge, better known as a dielectric barrier discharge (DBD), which, due to a lack of sparks and streamers, produces minimal audible noise. Figure 1 shows that DBDs are made by insulating either one, both, or part of the electrodes with dielectric material, most commonly fused silica glass or plastics. System performance strongly depends on the frequency of the applied voltage and the working gas. DBD plasmas typically range from 1-100 kV, and result in

many filamentary discharges. The electrons remain on the dielectric surface and oppose the external electric field, resulting in short lived streamers with lifetimes ranging from 1 to 10 ns [12].

1.1 Applications and Characterization of CAPs

The wide range of CAP induced effects has motivated interest in multiple applications in bioscience and agriculture; however, system optimization requires elucidating the plasma properties and mechanisms involved. The voltages applied and the timescale of ion recombination, which can be on the order of hundreds of nanoseconds [13], hinder direct measurement of the plasma species by physical sampling. One can use optical emission spectroscopy (OES) and optical absorption spectroscopy (OAS) to assess the light emitted and absorbed, respectively, to discern the chemical components over a specific time range in the bulk of the plasma or at a specific location [14].

Experiments studying DC corona discharges in air show that humidity plays a key role in increasing ozone generation, which alters plasma chemistry, while leaving the electron distribution unchanged for relative humidity up to 100% [15]. Plasmas can also abate volatile organic compounds through catalytic reactions involving oxidative species and photocatalytic reactions [16]. Ozone generation can also reduce microbial population in spinach, although it did discolor the leaves [17]. Applying the same system to *Bacillus atrophaeus* in a sealed package deactivated the spores after 60 s of treatment [18]. Three to five minute dielectric barrier discharge (DBD) treatment yielded 99.93% germicidal

efficiency for *E. coli* [19] with temperatures below 43 °C, which is well below the threshold for thermal inactivation.

CAPs offer a novel method for sterilizing medical instruments [20], enhancing wound healing [21], enhancing food safety and shelf-life [22], and treating cancer [23]. Recent studies have demonstrated that CAPs effectively eliminated bacteria and the remaining microscopic remnants on surgical equipment such as scalpels and forceps [24]. CAP treatment of open wounds leverages similar bactericidal effects to reduce the risk of hospital acquired infections [25]. CAPs induce these effects by ions and charged radical chemical species bombarding the cell surface [26,27]. These same radical species and ions can also treat food products to eliminate microorganisms to promote food safety or shelf-life extension [27,28]. CAPs can avoid the side effects of current sterilization methods, such as chlorine washes and pasteurization, which potentially leave traces of carcinogens or alter the taste and texture of food due to heating and chemical toxicity [29]. The absence of induced bulk heating allows CAPs to maintain texture and flavor [30]. The athermal nature of CAPs enables application to numerous materials, ranging from metals to plastics [9].

1.2 Indirect and Direct Application of Plasmas to Samples

One may characterize plasma delivery to a sample in one of three ways based on the current flow in the system [23]. Direct plasma treatment involves applying current directly to the sample, such as when the treated surface acts as an electrode as in Drexel’s

floating electrode dielectric barrier discharge [31]. Indirect treatment entails generating the plasma between two electrodes away from the sample surface and then propelling it toward the surface. The final method is a hybrid approach that generates plasma using a mesh electrode and then flows the species onto the surface without delivering current to the sample.

Dielectric barrier discharges (DBDs) offer high power application compared to other discharge methods with limited material and electrical requirements for multiple applications [32]. Argon and carbon dioxide DBDs effectively inactivated *Lactobacillus sakei* and *Photobacterium phosphoreum* on agar slab samples [33]. A two-minute 14 kV discharge induced a 5 log reduction in *Lactobacillus sakei* population and a 6 log reduction in *Photobacterium phosphoreum*. OES showed the generation of atomic oxygen, N_2^+, OH, and N radical species at room temperature. Observing these effects begs the question of what specific plasma parameters affect the sterilization and sanitization process.

Spatial and temporal behavior of species within the gap may also impact treatment efficacy. Spatial and temporal evaluation of a DBD system with helium and impurities showed that gas ionization, and therefore radical species production, began at the anode [34]. OAS elucidated kinetic mechanisms for radical species formation and demonstrated that humidity played a key role in species generation but not in the plasma breakdown [35].

One can also construct flowing DBDs, which were investigated for N_2 at atmospheric pressure [36] to sterilize small packages by flowing gas through narrow openings or polymerize a microcapillary [37]. These applications would be considered indirect treatments since the species are propelled toward the surface using flowing gas. This technique could also sterilize equipment without costly disassembly and down time.

Analogous to flowing DBDs, one can also apply plasmas to biological specimens by using plasma jets, in which the plasma is formed away from the target and subsequently propelled (or blown) toward the target [38]. Figure 2 shows a typical plasma jet design.

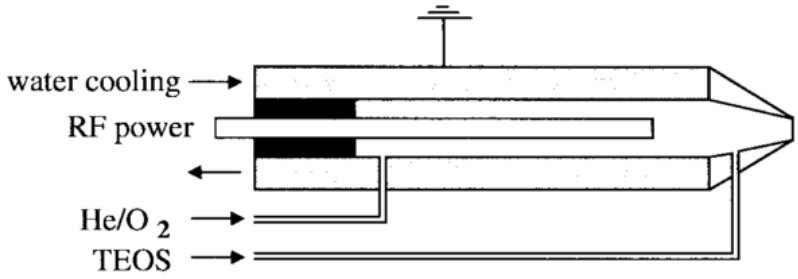

Figure 2: Typical plasma jet configuration from [38]

The jet properties were explored when applied to a surface and not applied to a surface at all, allowing the species to interact with the bulk gas and surrounding medium. Ambient conditions and the gas used for the discharge influenced the species generated. Similar in nature is the cold plasma torch that is generated using an RF source, as shown in Figure 3.

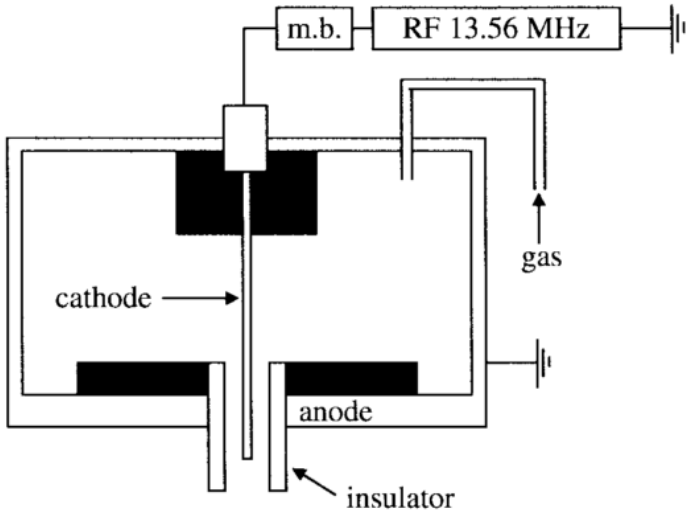

Figure 3: Cold plasma torch schematic from [38].

An inexpensive plasma jet can be used to produce the same chemical species as more expensive setups [39]. OES measurements of the breakdown characteristics of a plasma jet showed that the applied current strongly influenced the discharge regime and electron, ion, gas, rotational, and vibrational temperatures [40]. Jets inducing biocidal effects have also been characterized by OES [41]. Carefully calibrated monochromator measurements of various species, such as atomic oxygen, ozone, and UV emission showed that UV emission greatly exceeded U.S. Environmental Protection Agency requirements for sterilization [41]. Thus, sterilization resulted from a combination of the species and UV radiation. The interaction of the jet with the surrounding ambient air strongly influenced ozone and atomic oxygen generation. Electrical and OES measurements for similar experiments with helium yielded similar results [42].

Indirect application has also been studied for treating agricultural specimens and extending shelf life. Flowing air through a microwave induced plasma device and allowing the gas species to flow indirectly onto a sample of pork reduced bacterial colonies [43]. Two 2.5 min treatments were enough to maintain the microbial load to the detection limit of 10^2 CFU/g for a period of 20 days while stored at 5 °C. Another study examined indirect plasma treatment of chronic wounds with active bacteria colonies [44]. Daily 5 min treatments with a 2.46 GHz, 86 W microwave plasma device flowing argon gas at 2.2 slm reduced wound healing time of diabetic foot disease by half. Pain in the associated limb also decreased within five days of treatment.

1.3 OES Background

OES measures the light emitted by a system and extracts information about the particles in the system through various analytical techniques. Every element can be excited and then de-excite by emitting energy in some form or another. When excited electrons return to a lower energy level, energy can be released in the form of various wavelengths of light, which can then be separated by a spectrometer using a grating that acts as a prism. The grating separates the light into its various wavelengths, which are directly related to the properties of the particular species. Over time, many techniques have been developed to extract information about the particles emitting the light [45–47]. One commonly used technique uses the Boltzmann equation, to relate the population of different excited energy levels to the temperature by

$$\frac{N_j^Z}{N^Z} = \frac{g_j \exp\left[-\frac{E_j^Z}{kT}\right]}{U^Z(T)}, \tag{1.1}$$

where N_j^Z represents the population densities of the excited energy levels as a function of temperature T [48], the superscript Z represents the ionization stage, N^Z is the number density, E_j^Z and g_j are the energy and degeneracy levels, respectively, $U^Z(T)$ is the partition function, an k is Boltzmann's constant. The Saha equation relates densities of ionized species to temperature by

$$\frac{N_e N^Z}{N^{Z-1}} = \frac{2U^Z(T)}{U^{Z-1}(T)}\left(\frac{2\pi mkT}{h^2}\right)^{3/2} \exp\left(-\frac{E_\infty^{Z-1} - \Delta E_\infty^{Z-1}}{kT}\right), \tag{1.2}$$

where N_e is the electron number density, E_∞^{Z-1} is the ionization energy of the Z-1 species, ΔE_∞^{Z-1} is the plasma correction for the ionization energy, h is Planck's constant, and m is electron mass [48]. The applicability of the Boltzmann equation relies on the electrons and ions being at local thermodynamic equilibrium (LTE). Thermodynamic equilibrium requires that the temperature from the Saha and Boltzmann equations must equal the Maxwell-Boltzmann distribution of the free electrons [48], which requires

$$N_e \geq 10^{12} T^{1/2} (\Delta E)^3 \text{cm}^{-3}, \tag{1.3}$$

where ΔE is the energy gap difference between the transition levels and T is the temperature of the equilibrium radiation field [48]. These equations and equilibrium principles are utilized in many modern spectral fitting codes. They automatically generate a synthetic spectrum and then alter the parameters of the equations to obtain a best fit to measured spectra. These types of codes are utilized in the work of this thesis and will be discussed in more detail in Chapters 2 and 3 as well as in Appendix A.

One determines the electron density from the intensity shifts produced by Stark broadening [48]. Molecules also have excited states that can emit light that one can use to determine particle temperatures. Molecules exhibit various rotational, vibrational, translational, and electronic excited states. The emission from these states can be fit to calculated spectra using various fitting routines either calculated by hand or in software [48].

OES is a powerful tool that has been applied to many different plasma applications [49–51]. One experiment developed a new method of determining relative concentration of reactive particles [52]. Monitoring the emission peak intensities of the reactive species and select noble gases allows relative species concentrations to be monitored as one alters plasma parameters [51]. Accurately determining the electron temperature and electron energy density function required carefully reviewing the calculation methods and the accepted electron impact excitation cross sections while developing correction factors to obtain better spectral fits and density calculations. The partial local thermal equilibrium (PLTE) model was validated for a 25 kHz, 15 kV, 2 W plasma jet and then used to map electron temperatures in the jet plume [53]. A fused silica tube, with a center ground electrode and ring high voltage electrode, generated a plasma jet and was analyzed using OES. The Boltzmann plot showed that the maximum electron temperature was 1.0 eV with a gas temperature of 100°C. Ambient air leaked into the system and was ionized, contributing additional species to the argon emission spectrum. OES showed that applying 3 to 4 kV to a thin stainless steel electrode inserted into a Pyrex capillary and flowing either helium, argon, or oxygen through the tube

created a plasma jet that produced reactive species when applied to liquid water [54]. OES further demonstrated that changing the gas flowed in the capillary changed the gas temperature. For instance, the temperature ranged from 400 K for helium to between 3000 K and 4000K for argon and oxygen. The electron densities calculated using Stark broadening were on the order of 10^{21} m^{-3} for helium and 10^{22} m^{-3} to 10^{23} m^{-3} for oxygen and argon. A plasma jet was generated in a quartz tube using 12.2 to 17 kV to study the effects of the species generated in an argon/water mixture [55]. Using axially and spatially resolved OES to determine the rotational temperature using Boltzmann plots showed that the gas temperature increased with water concentration in the inlet gas. The temperature ranged from 625 K for pure argon to 1125 K for 0.76% water to argon. The OH radicals achieved a maximum at 0.05% water in the argon/water vapor.

A quartz syringe was used to form a plasma jet to study the breakdown when generated using DC and AC voltages [56]. Spatially resolved OES showed the effects of using up to 10 kV of DC voltage or up to 30 kV peak to peak of an AC source. The plasma plume generated with DC was approximately twice as long as that generated with AC. The DC generated discharge also had current that was about two orders of magnitude larger than the AC discharge. The intensity of the OES spectra for the DC discharge was much higher than for the AC discharge. Synthetic spectrum fitting showed that the rotational temperature of the AC plasma was 30 K higher than the DC plasma. Using OES for another plasma generated using a quartz capillary in water gave the electron densities by finding the Stark broadening of the H_β lines and temperatures were found by the Boltzmann plot method [57]. For conductivity below 45 μS cm^{-1}, the

discharge occured in the liquid stage with a rotational temperature of 1900 $\pm$ 200 K. For conductivities above 45 μS cm^{-1}, the discharge took place in a bubble with a rotational temperature of 1600 $\pm$ 200 K. The electron density was 10^{21} m^{-3} for the liquid discharge while the electron density was 10^{20} m^{-3} for the bubble discharge.

1.4 Thesis Purpose and Purview

Despite numerous studies on jet and DBD discharges, few studies have addressed higher voltages above tens of kilovolts. Studies of a DBD discharge on a dielectric surface at 8.5 kV showed that oxidation, nitridation, and carbonization into glass surface occured after the DBD treatment [58]. Applying a 15 kV DBD plasma to *E. coli* showed a 1.5 log reduction for a 5 min exposure [28]. Further studies at 56 kV and 70 kV examined bactericidal effects, but not the effect of the container material [35]. The effects of the plasma species on bacteria were well characterized but the effect of the plasma on the material must be understood at these voltages.

While many groups use “high voltages” to generate CAPs, the actual threshold at which one attains a high voltage CAP (HVCAP) is somewhat ambiguous. For this purpose, we define HVCAPs as CAPs generated with voltages above 20 kV. The higher applied voltage increases the electric field for a given gap distance, potentially changing the excited species produced. The effects of the higher voltage on species generation and packaging materials remains unclear. The key issue for applying HVCAPs for treatment of sealed packages involves the interaction of the electric field and plasma species with

the packaging material. Specifically, do the plasmas alter the packaging material to release chemical species, do the materials alter OES and OAS measurements, or some combination of the two? The polymers in plastics can undergo changes when exposed to plasma discharges [59]. Plastics are known UV absorbers [60], altering the spectra obtained by either OES or OAS.

This thesis elucidates the effect of higher voltages on plasma generation using a DBD system. The work has two main thrusts: (1) Assessing the impact of food packaging materials on plasma species generated and detected within the containers and (2) Examining the change of plasma species while varying applied voltage from 30 kV to 90 kV. OES was performed to extract information about rotational temperatures represent the gas temperature in DBD type discharges. This data was analyzed by fitting a synthetic spectrum software called SPECAIR (SpectralFit S.A.S., Antony, France). This software estimates rotational, vibrational, translational, and electronic temperatures by fitting an artificial spectrum generated from available models of plasma discharge to the measured spectrum. The fit is then used to modify the model emission and estimate the plasma temperature.

To examine the impact of the packaging materials, we conducted experiments using three different plastic containers and bags that are representative of the materials used in the food industry. We also selected common gases used in the food industry, namely dry air, humid air, helium, and nitrogen. This also allowed for direct benchmarking to previous work [17,18,28]. The spectra obtained were then analyzed using SPECAIR to

obtain the rotational temperatures. Current and voltage measurements yielded the power absorbed by the plasma so that variation with working gas could be determined. Lissajous diagrams, which parameterize the system with applied voltage, were created to calculate various electrical properties and characterize the plasma for each type of gas used [39,61]. This provides a means to calculate various properties such as power dissipated in the plasma, capacitance of the gap, and capacitance of the dielectric. This allows for a parameter space mapping of the DBD discharge to optimize the plasma for different applications.

The second half of this thesis explores the effects of voltage on plasma species generation. A high resolution spectrometer was utilized to better characterize species with low concentrations and slight changes in species concentration that arise due to changing voltage. Voltage and current measurements were again performed to examine the power dissipated by the gas for each voltage setting while using helium gas.

CHAPTER 2. CHARACTERIZATION OF HIGH VOLTAGE COLD ATMOSPHERIC PLASMA GENERATION IN SEALED PACKAGES AS A FUNCTION OF CONTAINER MATERIAL AND FILL GAS

2.1 Experimental Setup

Figure 4 shows a schematic and circuit diagram of the experimental system. The DBD system consisted of two 3 mm thick high density polyethylene sheets (IKEA, Sweden), which serve as dielectrics, on the top and bottom of a polypropylene container with dimension of 4.4 cm by 26.7 cm by 17 cm. The bottom and sides of the container were 0.12 cm thick and the top was 0.19cm thick. We contained the plasma and gaseous species generated during treatment with B4170 standard clear plastic food storage bags (Barrier Bag, Standard Air Corporation, Duncan SC, US) typically used for vacuum food storage. We connected a Phenix BK 130 Dielectric test set (Phenix Technologies, Accident, MD, USA) to two 6 in diameter aluminum disk electrodes placed on the top and bottom of the container. The Phenix system takes an input of 120 Volts at 60 Hz and outputs up to 130 kV with currents on the order of milliamperes.

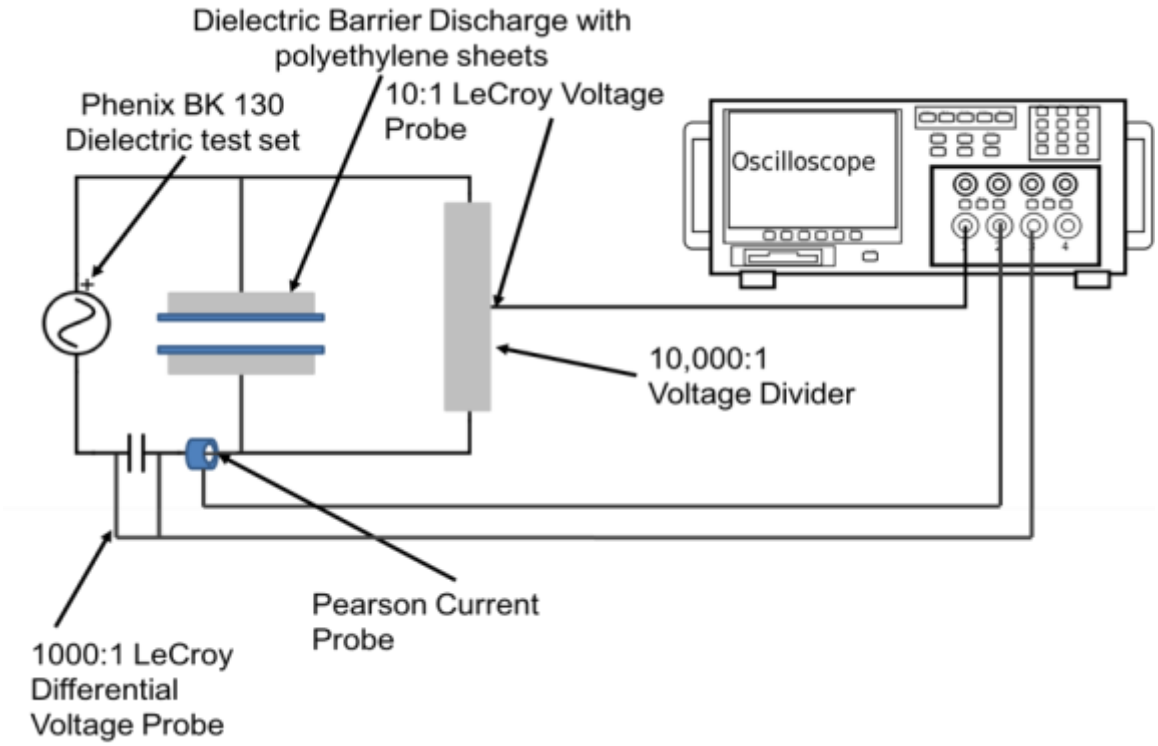

Figure 4: Circuit schematic of the experimental setup for plasma generation and diagnostics.

The electrical measurements were recorded using a LeCroy Waverunner 6zi oscilloscope (LeCroy, Chestnut Ridge, NY, USA) connected to a 10,000:1 Nicrom-Electronic voltage divider (Nicrom-Electronic, Novazzano, Switzerland) and a Pearson Rogowski coil (Pearson Electronic, Palo Alto, CA, USA). Two LeCroy voltage probes (10:1 and 1000:1) were used to measure voltages across a capacitor and at the output of the voltage divider. The current probe and voltage divider were connected in parallel, running the output of the high voltage supply through the current probe. We connected a voltage divider directly to the output and the system ground to measure input voltage and across the top and bottom electrodes to measure the potential across the sample container, keeping it in parallel with the system.

We used an OceanOptics HR2000+ spectrometer to collect spectroscopy data. All background light was subtracted from the spectra using the OceanOptics OceanView software wizard for emission spectroscopy. The spectrometer used a custom made fiber optic cable with a 400 μm opening with PEEK DSMA connectors. A 200-2000nm UV-VIS collimating lens focused the light from the plasma onto the fibers of the cable. The lens was coated in Teflon tape to prevent arcing during plasma generation. We ran OceanView software on a Microsoft Surface to allow for portable use of the spectrometer. We aligned the fiber optic probe using an OceanOptics SPL-1DH Deuterium-Halogen light source. Once aligned, we taped the probe 4.5 cm from the edge of the container to maintain alignment throughout data acquisition.

2.2 Methods

The OceanOptics spectrometer requires a 30 s exposure time to obtain spectra due to the diffuse nature of our plasma. The OceanOptics HR2000+ is a Charge Coupled Device (CCD) sensor for taking the spectra. We took a series of spectra with and without a light source to optimize the averaging of the exposure time and then measured the background and signal to noise ratio. Averaging six 5 s scans gave the highest signal to noise for the plasma generated in the experiments.

We used OES to determine how the container and bag material impact OES measurements and species generation. To assess the bag effect, we generated ambient air plasma in a container in two different ways. The first method used a plastic container

with a hole drilled in the side that is not sealed in a bag. This allowed for direct observation of the plasma through the container, effectively eliminating the influence of the container material on the recording itself. The second method assessed the impact of the container on the measurement by generating the plasma in the container sealed in a bag while still taking the spectra through a hole. We compared the spectra by analyzing the peak intensity for the N_2 2^{nd} positive system to establish a reproducible peak across all conditions. We wrote a MATLAB script that took the raw OES data and gave a list of peak intensity and its corresponding wavelength. We also analyzed the species between runs (within the resolution of our spectrometer) to ensure consistency of the plasma. We accounted for experimental variation by collecting three measurements and averaging them to obtain the wavelength and intensity for the peaks and determined the error bars by taking the standard deviation of the three measurements.

2.3 Results

We first performed OES measurements to assess the effect of the plastic container material in the container on the emission spectrum. The intensity of the peaks decreased across the measured wavelength range with no wavelength shift. Figure 5 shows representative spectra for the of ambient air plasma at 72 ± 3.7 kV RMS to assess the decreased intensity of the spectrum. Repeating the experiment three times showed that the plasma composition remained consistent for repeated experiments. Table 1 shows the peaks identified, which did not change composition by introducing the container.

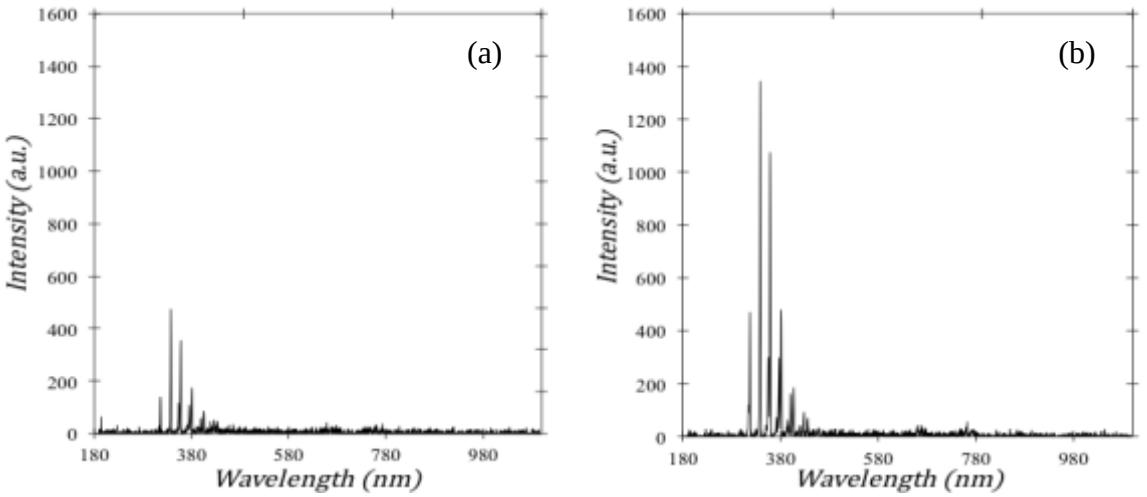

Figure 5: Representative spectra of ambient air plasma at 72 ± 3.7 kV RMS from Container 1 measured (a) indirectly and (b) directly through the container material, demonstrating that the container altered the intensities of the peaks, but not the wavelengths, which correspond to the species generated.

Table 1: Species identified from Figure 2 present in both spectra (a) and (b).

Wavelength (nm)	Species
316.102	N_2
337.453	N_2
353.665	N_2
357.829	N_2
375.391	N_2
380.469	N_2
399.828	N_2
405.812	N_2
426.953	N_2+

We also benchmarked the containers against each other to account for variation in the material by comparing the intensity of the three most intense peaks across the three containers in Figure 6. The error bars demonstrate the reproducibility of the measurements for a given container.

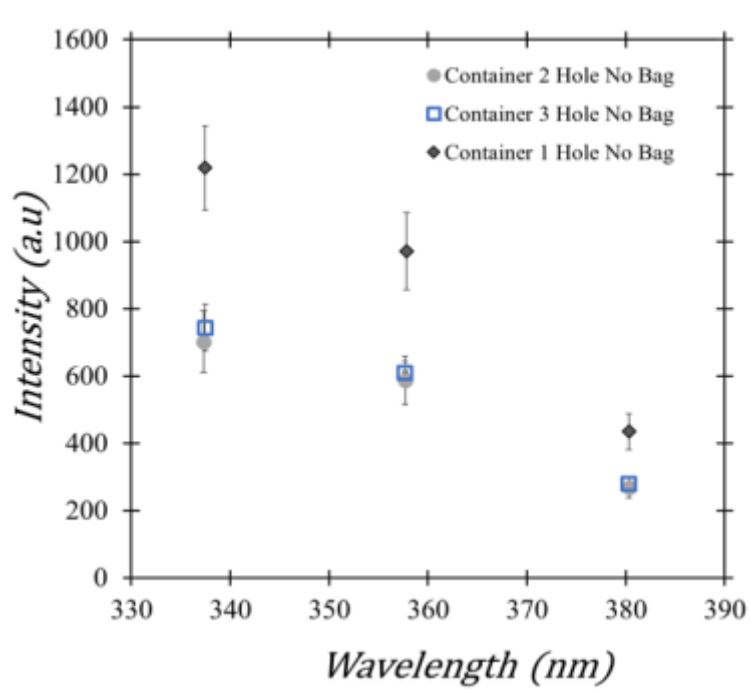

Figure 6:Comparison of peak intensity for directly observed 72 ±3.7 kV RMS ambient air plasma showing reproducibility between containers.

As is typical of OES, slight variations arose in the peak intensity of the spectra. Despite maintaining ambient conditions, such as pressure and temperature, we observed intensity variations that were consistent across all the tests. Numerous other factors not easily controlled can also impact gas breakdown, such as humidity of the ambient air [62]. Thus, we consider variations of intensity for relative comparisons between averaged peak intensity data. One of the three containers exhibited higher intensities than the others, which we attribute to minor variances in the transparency of the plastic container. The

consistency of the distortion across all wavelengths permitted correction in subsequent analyses. Examining relative intensity and relative peak heights across the spectrum allowed qualitative comparison of plasma generation.

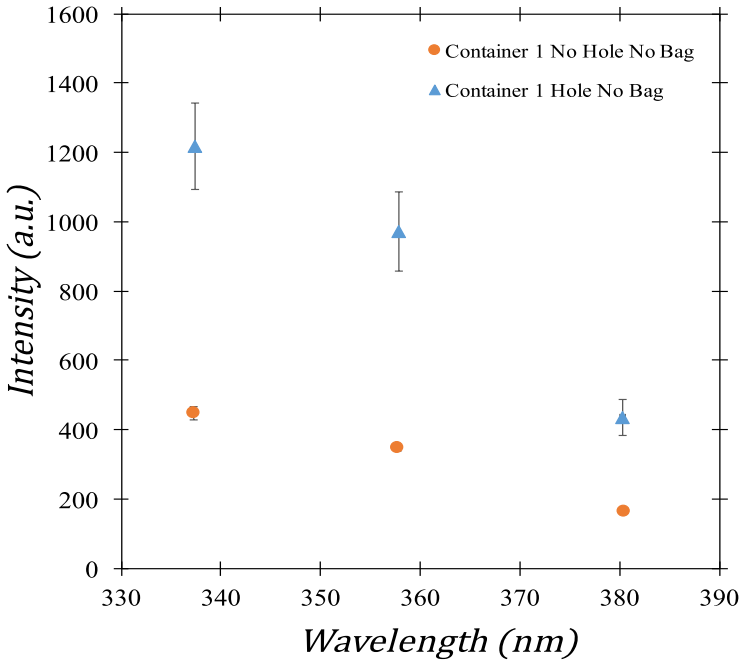

Figure 7: Comparison of peak intensities for plasma observed by direct line of sight and through container material showing that the container decreased intensity by an average of 63.1% $\pm$ 0.94%.

Figure 7 demonstrates the impact of the container by comparing the intensity of the three most dominant peaks in an ambient air spectrum by either measuring through the container or through a hole in the container. Figure 7 shows that the container material decreased the intensity by an average of 63.1% $\pm$ 0.94% for each peak across the measured spectra, allowing a direct comparison of the two spectra. We observed no change in molecular species of the plasma in the spectra as evident by minimal change in the wavelengths corresponding to these peaks.

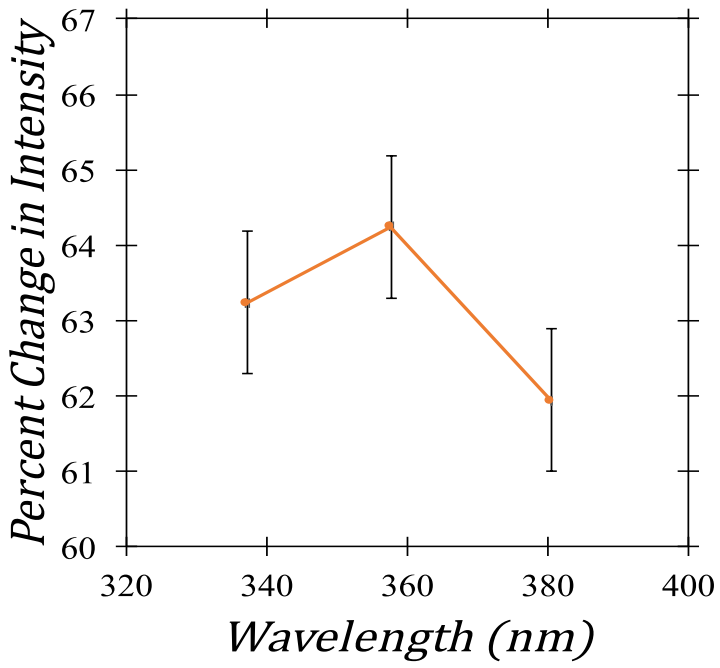

Figure 8: Percent change in intensity of peaks, showing the container decreased peak intensity by an average of 63.1% ± 0.94%.

Figure 8 indicate that the container material simply serves as a broadband absorber. The change in intensity for each peak varies between 61.9% 63.2%, and 64.2% with a standard deviation of 0.94%. This slight change in intensity can be considered uniform for our purposes. This means that the container material will not affect the ratio of the peak intensities, preserving any detail that can be obtained from fitting.

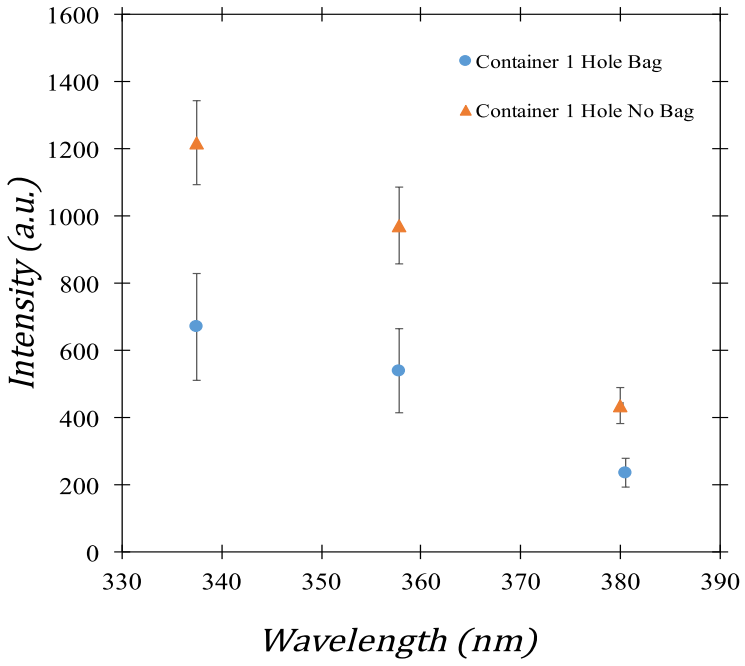

Figure 9: Intensity variation of spectra peaks with and without a plastic bag sealing the container showing the plastic bag reduced intensity by an average of 44.8% ± 0.49%.

We next performed the same measurement with the container sealed in a plastic food grade bag typically used for storage with vacuum sealers to assess the impact of the bag on species generation. Figure 9 shows the variation of intensity between the OES measurements conducted through the bag or without the bag. As for the container, the bag reduces the intensity with no observable change in wavelength. Figure 10 shows that the intensity of the three most intense peaks observed with and without the plastic bag material changed by an average of 44.8% ± 0.49% across the entire portion of the spectrum we analyzed.

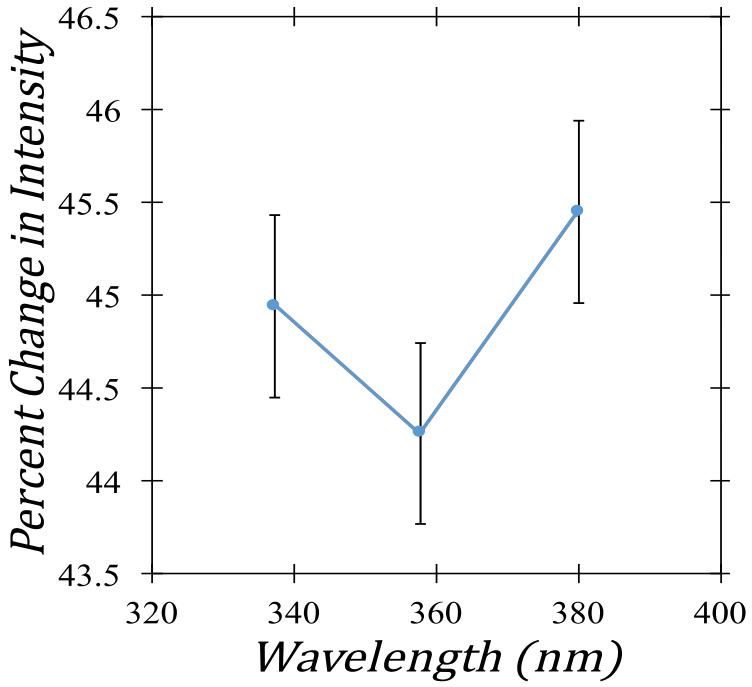

Figure 10: Percent change in intensity of peaks, showing the bag material decreased peak intensity by an average of 44.8% $\pm$ 0.49%.

The change in intensity for each peak varied between 44.9%, 44.2%, and 45.4% with a standard deviation of 0.49%. Again the slight change in intensity over the observed wavelength range can be considered uniform for our purposes. This means that the seal bag material will not affect the ratio of the peak intensities preserving any detail that can be obtained from fitting. Thus, the bag also acts as a broadband absorber with minimal change on species generation as demonstrated by minimal change in the wavelengths of the peaks.

Figures 5 – 10 showed that molecular nitrogen (N_2) emissions from 300 to 440 nm dominated the DBD spectra. We corrected all the spectra for background light and noise inside the CCD. The OceanView wizard for these corrections gave a signal to noise

ratio of at least 100:1 when gated at 5 s and averaged over six readings for a total of 30 s of plasma duration. Figure 11 shows a representative spectrum showing the N_2 band that dominates all peaks in the spectrum. This allows comparison of the N2 bands across all spectra measured.

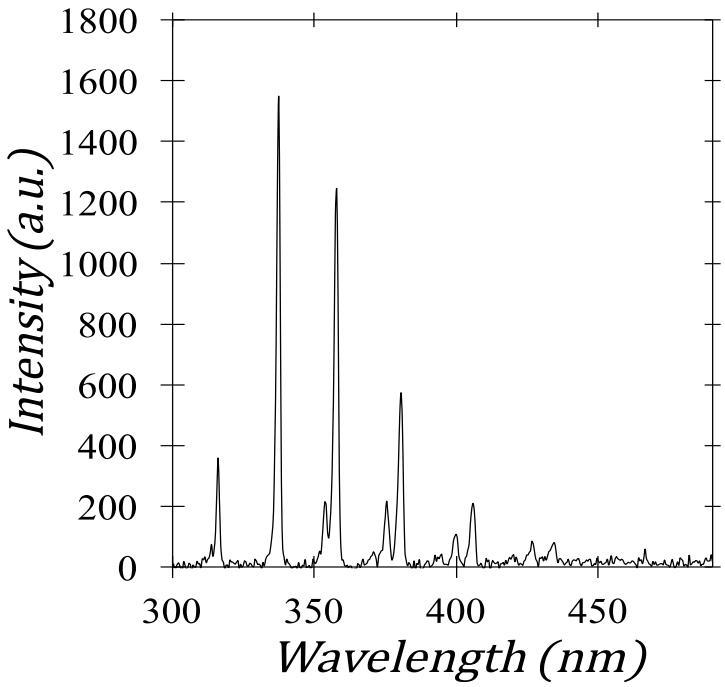

Figure 11: Representative optical emission spectrum for the dielectric barrier discharge system demonstrating nitrogen spectrum at 72 ± 3.7 kV RMS for a duration of 30 s.

We can also analyze spectra, such as Figure 11, to determine the rotational and vibrational temperatures using the SPECAIR 3.0 (SpectralFit S.A.S., Antony, France) fitting program. We chose nitrogen, helium, and compressed air as the fill gases for plasma generation. The nitrogen, helium and compressed air were obtained from the Purdue University Stores (West Lafayette, IN USA) in gas cylinders minimize the variability of the humidity and allow for controlled flushing of the containers.

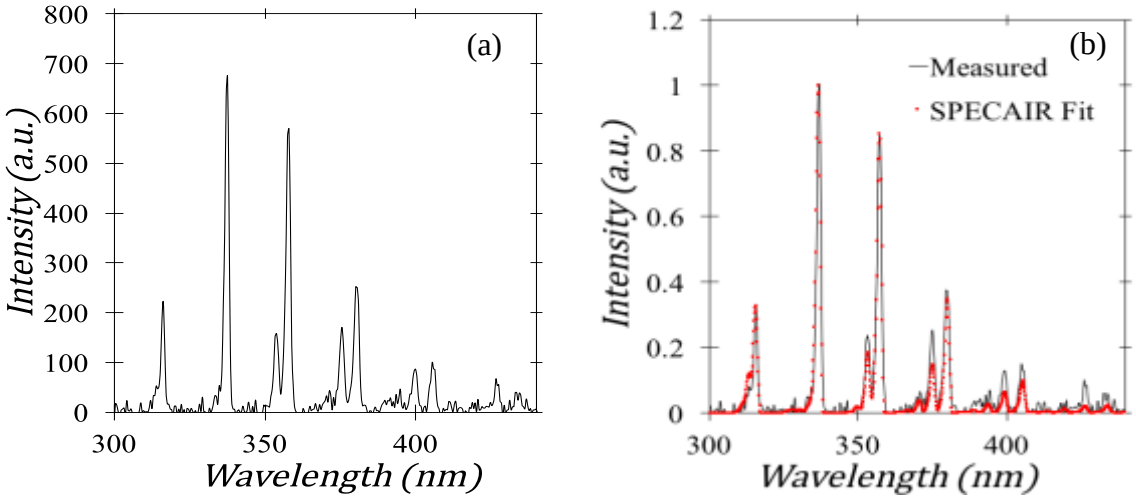

Figure 12: (a) Measured optical emission spectrum for a compressed air plasma generated with 80 ± 3.7 kV RMS and (b) the fitted spectra using SPECAIR.

Figure 12 shows the original spectrum obtained for the air plasma and the data fit in SPECAIR. The N_2 2nd positive system from 300 to 400 nm dominated the spectra, as shown by Figure 12 [63]. The presence of multiple states for the system facilitates the fitting of the vibrational temperature. Figure 13 repeats this analysis for the nitrogen discharge and again shows that N_2 2nd positive system dominates the spectra with no other transitions. Figure 14 shows that although helium peaks arise between 600 nm and 700 nm, the N_2 2nd positive system also dominates the helium discharge. We observed nitrogen peaks despite our best efforts to isolate the containers and flush with pure helium to purge the system of any air. We currently hypothesize that the nitrogen arises due to leakage of air into the container during the sealing process, particularly during the removal of the tubes used for flushing helium through the container. Previous assessment of a similar experiment showed that approximately 16% of a bag filled with helium contained air, resulting in the presence of nitrogen in the spectrum even though helium

was the gas used to fill the sealed bag [28]. Since nitrogen has a lower ionization energy than helium [64,65], it will ionize more easily at lower applied voltages and will dominate the spectrum. Although a pure helium environment would be ideal for scientific assessments of the impact of fill gas, the actual measurement condition containing nitrogen likely better represents more relevant conditions for treating food products in an industrial environment.

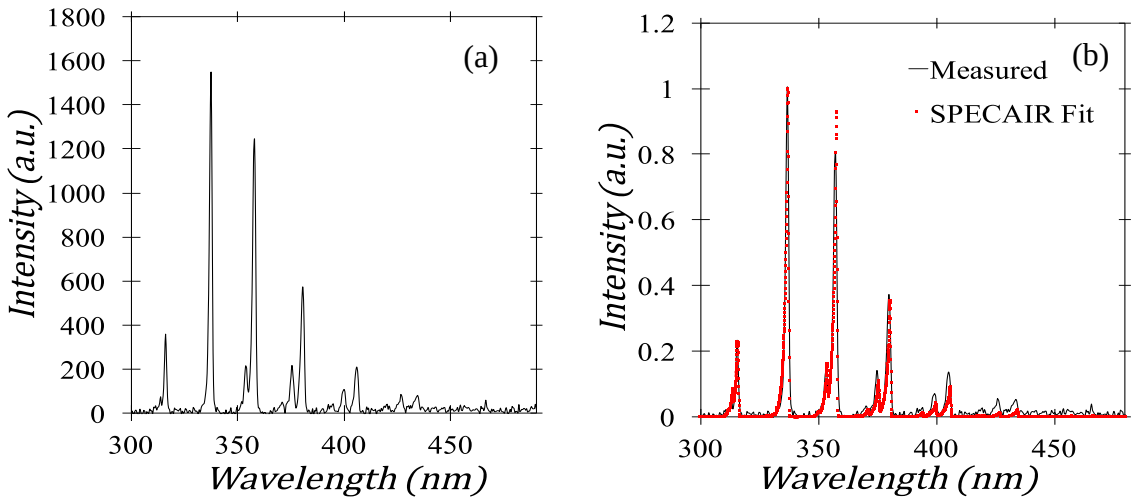

Figure 13: (a) Measured optical emission spectrum for a nitrogen plasma generated at 72 ± 3.7 kV RMS and (b) the fitted spectra using SPECAIR.

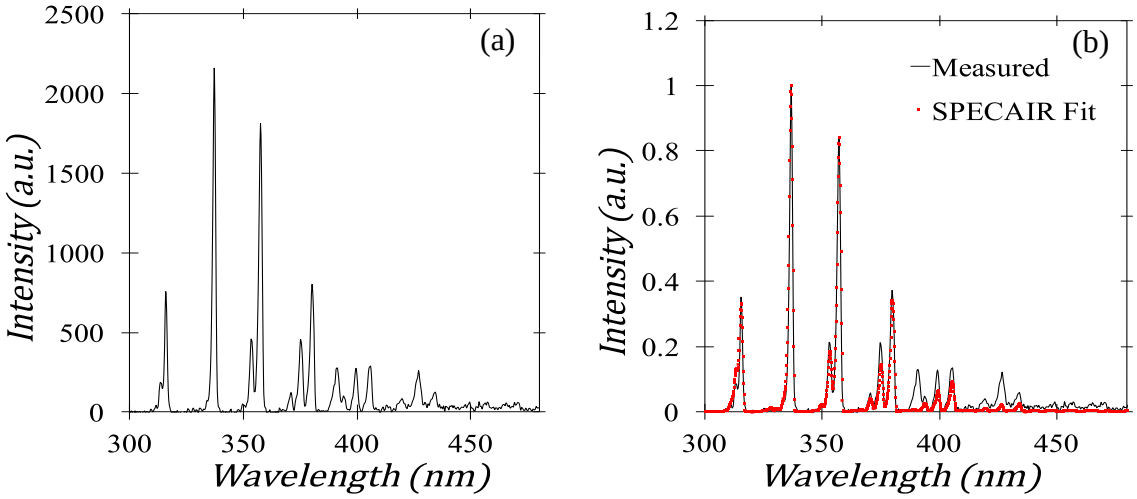

Figure 14: (a) Measured optical emission spectrum for a helium plasma contaminated with air generated at 37 ± 3.7 kV RMS and (b) the fitted spectra using SPECAIR. Note the presence of nitrogen is due to the flushing method used for the bag container setup.

Table 2: Translational (T_{trans}), vibrational (T_{vib}), and rotational (T_{rot}) temperatures calculated using SPECAIR for nitrogen, helium, and compressed air plasmas.

Gas	T_{trans} **(K)**	T_{vib} **(K)**	T_{rot} **(K)**
Nitrogen	1088 ± 100	2025 ± 100	415 ± 100
He	1307 ± 100	2323 ± 100	479 ± 100
Compressed Air	1431 ± 100	2303 ± 100	385 ± 100

Table 2 shows the translational, vibrational, and rotational temperatures of the tests for nitrogen, helium, and compressed air as fill gases. The rotational temperatures ranged from 479 ± 100 K for helium to 285 ± 100 K for compressed air. Translational temperatures ranged from 1088 K for nitrogen to 1421 ± 100 K for compressed air. This

is in contrast to values obtained in previous work conducted at 15 kV, showing the translational temperature to be 300 ± 100 K [28]. This suggests that the higher voltage impacts the energy of the species produced.

We next considered waveforms for compressed air, atmospheric air, nitrogen and helium to compare power dissipated in different plasmas. Figure 15 shows the electrical measurements when the container is sealed with a food grade vacuum seal bag and then flushed with compressed dry air.

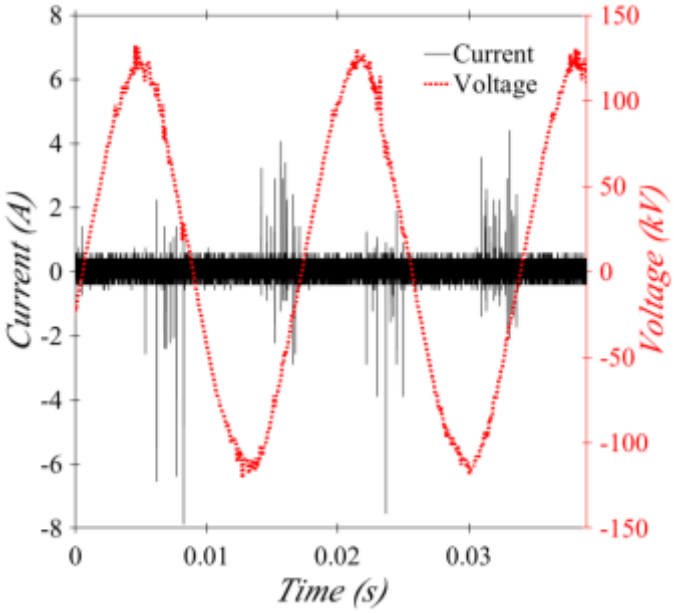

Figure 15: Measured voltage and current for a compressed dry air plasma generated at 80 ± 3.7 kV RMS.

The voltage was measured to be 80 ± 3.7 kV RMS with current peaking around 7.88 mA. The current and voltage exhibited the filamentary discharge expected of the DBD

[11,66,67]. Figure 16 shows the electrical measurements for helium, nitrogen, and ambient air DBDs. Current spikes 90° out of phase with the voltage change still arise.

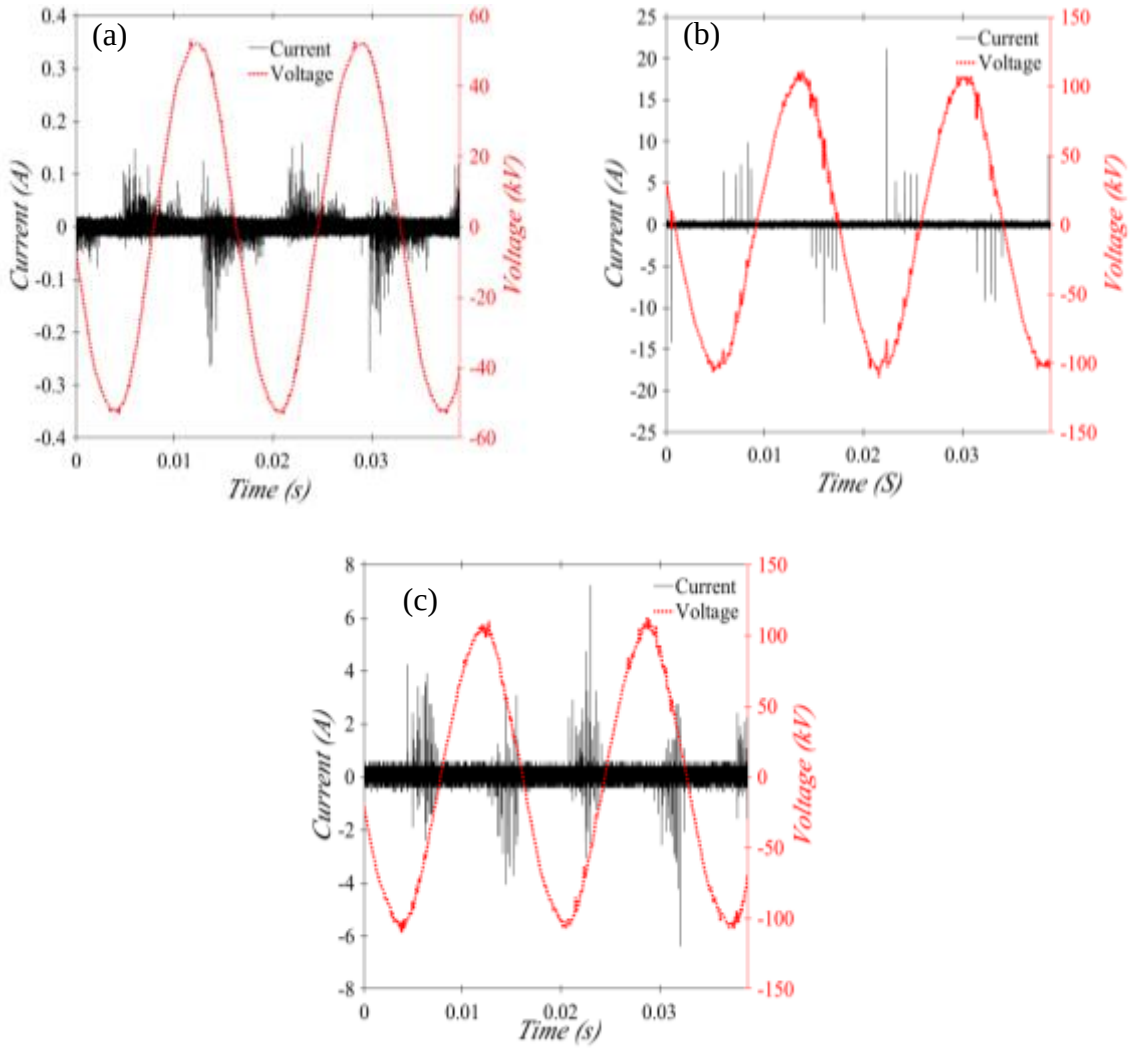

Figure 16: Voltage and current waveforms for (a) helium at 37 ± 3.7 kV RMS, (b) nitrogen at 72 ± 3.7 kV RMS, and (c) ambient air at 72 ±3.7 kV RMS.

We can then use the voltage and current measured across the discharge gap and a capacitor in series with the gap, as shown in the circuit diagram in Figure 4, to generate Lissajous diagrams to further elucidate the power dissipation by these various plasmas [68]. One obtains a Lissajous diagram by plotting the applied voltage as a function of the

voltage measured across the capacitor to create a parallelogram that represents various properties of the discharge. The change in the slope of the sides of the parallelogram indicates a change in capacitance, or charge transfer [68]. The power dissipated by the plasma is given by

$$P=CSf, \tag{2.1}$$

where the capacitance of the series capacitor, C, and the AC frequency (f = 60 Hz) are fixed, allowing the comparison of power dissipated by using the ratio of the plot area S of the various gases. Figure 17 shows the Lissajous diagrams for ambient air, compressed air, nitrogen, and helium plasmas. The slope and area remain relatively constant across the different gases except for helium, which has an elongated shape indicating a change in the gap capacitance of the DBD. This also suggests that residual charged species are left in the gap after the microdischarges have extinguished [69].

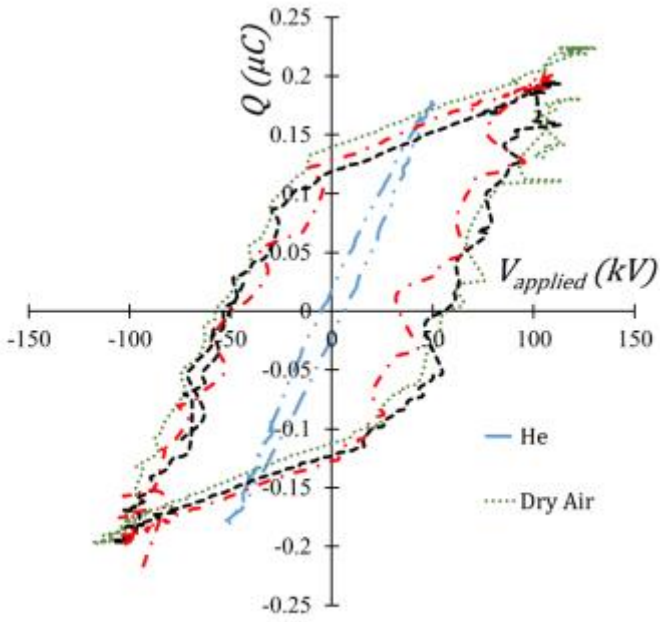

Figure 17: Lissajous figure showing changes in power dissipation and charge transfer characteristics for different gases.

Table 3: Power dissipated in the plasma for the different gases.

Gas	Power Dissipated (W)
Compressed Air	0.334
Nitrogen	0.288
Helium	0.0252
Ambient Air	0.284

Table 3 shows that the compressed air dissipated the most power while the helium dissipated the least. This can be attributed to not controlling ambient humidity during the

experiment. To better compare these values we looked at the percent change in the power dissipated and evaluated the slope of the side of the parallelogram.

Table 4: Percent change in power dissipation as compared to compressed dry air.

Gas	% Change in Power Dissipation	% Change in Slope
Nitrogen	-13.76	12.72
Helium	-92.44	-12.36
Ambient Air	-14.92	36.00

Table 4 compares the area and slope of the Lissajous parallelogram for nitrogen, helium, and ambient air to compressed air. The helium discharge dissipated approximately 92% less power than the air and nitrogen plasmas. The nitrogen and ambient air plasma varied from compressed dry air by 13.76% and 14.92%, respectively, exhibiting the effect of ambient humidity on the discharge. Nitrogen, ambient air, and compressed air have similar measurements because nitrogen is the most abundant constituent for these gases. Helium has a higher ionization energy than nitrogen [64,65], meaning that less of the applied power will go into the discharge and more will go into ionizing the ground state helium. This suggests that more of the power of the device is being used to ionize the helium than actually going into producing reactive species. Reactive species are needed to produce the sterilizing effect, so the reduction of these would be seen as a determent to using helium mixtures for treatment. A more in-depth study is needed to quantify the reduction of the species, to determine the potential impact to the sterilization efficacy.

CHAPTER 3. CHARICTERIZATION OF EFFECT OF HIGH VOLTAG ON PLASMA GENERATION

3.1 Experimental Setup

As in the setup from the initial OES experiments outlined in Chapter 2, two 3 mm thick high density polyethylene sheets (IKEA, Sweden), served as dielectrics. They were placed on the top and bottom of a polypropylene box with dimensions of 4.4 cm by 26.7 cm by 17 cm. The bottom and sides of the box were 0.12 cm thick and the top was 0.19cm thick. The plasma and gaseous species generated during treatment were contained with the same B4170 standard clear plastic food storage bags (Barrier Bag, Standard Air Corporation, Duncan, SC, US). We applied 60 Hz voltage using the Phenix BK 130 Dielectric test set (Phenix Technologies, Accident, MD, USA) to two 6 in aluminum disk electrodes placed on the top and bottom of the box. Figure 18 shows a schematic and circuit diagram of the experimental system used to elucidate the effect of voltage on the discharge.

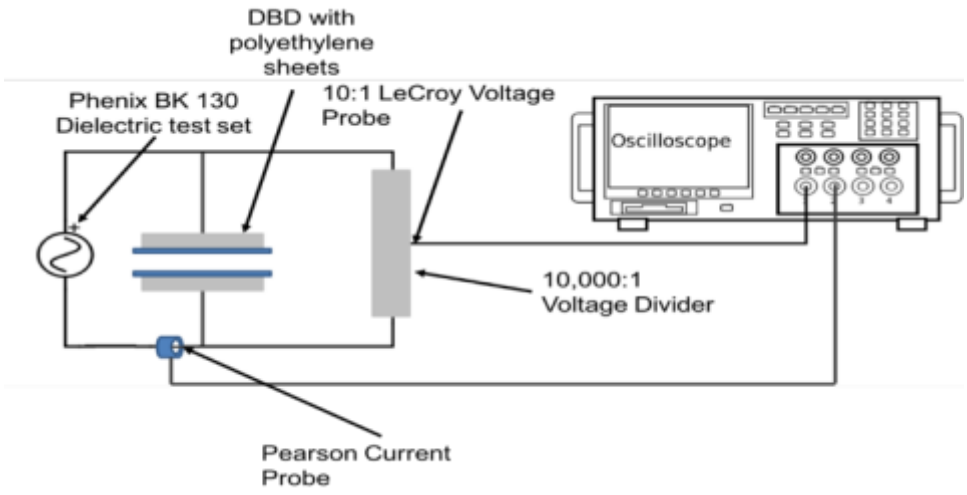

Figure 18: Circuit schematic of the experimental setup for plasma generation and diagnostics.

The electrical measurements were recorded using the same LeCroy Waverunner 6zi oscilloscope (LeCroy, Chestnut Ridge, NY, USA) connected to a 10,000:1 Nicrom-Electronic voltage divider (Nicrom-Electronic, Novazzano, Switzerland) and a Pearson Rogowski coil (Pearson Electronic, Palo Alto, CA, USA). The current probe and voltage divider were connected in parallel, running the output of the high voltage supply through the current probe. We connected a voltage divider directly to the output and the system return to measure input voltage and across the top and bottom electrodes to measure the potential across the sample box. The OES measurements were taken using a PI-MAX4 Intensified Charge Coupled Device (ICCD) (Princeton Instruments, Trenton, NJ, USA) with a timing resolution of 10 ps, a timing jitter of 35 ps RMS, an insertion delay below 27 ns, an internal timing generator from 0.05 Hz to 1 MHz, 1024×1024 imaging array, and less than 500 ps gating for high temporal resolution to enable effective background discrimination. We used a Princeton Instruments SP2500 (Princeton Instruments, Trenton, NJ, USA) spectrometer with a 500 mm focal length, and a 0 to 1400 nm scan range.

3.2 Methods

We applied 36.4, 44.8, 58.1, and 71.0 kV to generate a helium air discharge sealed inside of a container using the B4170 seal bags. We collected the light from the plasma using a fiber optic cable that was provided with the SP2500 spectrometer. The fiber was coupled to a 200-2000 nm UV-VIS collimating lens, which focused the light of the plasma onto the fibers of the cable. The fiber optic probe was aimed using an OceanOptics SPL-1DH Deuterium-Halogen light source to ensure that the lens collected light from the center of the diffuse discharge. We used a laptop running Lightfield software (Princeton Instruments, Trenton, NJ, USA) to interface with the camera and spectrometer to collect data from the ICCD. We used two different settings for the PI-MAX4 ICCD depending on the measurement. Spectra focused around 355 nm required setting a gain of 80 on the intensifier, a gate delay of 30 ns and a gate width of 1000 ms for six on chip accumulations. Larger “step and glue” sections of spectra ranging from 250 to 500 nm required setting a gain of 80 on the intensifier with a gate delay of 30 ns, and a gate width of 1000 ms for six on chip accumulations, each consisting of one exposure.

This study aims to elucidate how plasma species vary with the high voltages (from 36.4 to 71.0 kV RMS) typically used for this particular DBD setup by taking the same electrical and OES measurements [28,35]. We also sought to obtain higher resolution spectra to better observe rotational structure to more accurately calculate plasma temperature The spectrometer used the 1800 g/mm grating to maximize the

resolution while still transmitting enough light for ICCD detection. We obtain electrical and OES data simultaneously at 36.4, 44.8, 58.1, and 71.0 kV RMS and then processed it using custom MATLAB scripts (included in Appendix B) to obtain plots of the current and voltage, N_2 Second Positive system, spectra ranging from 250 to 500 nm to observe species generation, and text files that were fed into SEPCAIR (SpectralFit S.A.S., Antony, France) to obtain fits for rotational, vibrational, and translational temperatures.

3.3 Results

We first used the 1800 g/mm grating to assess the N_2 second positive system to obtain rotational temperature information for the plasma generated at each setting. Figure 19 shows a representative spectrum that was obtained and later fed into SPECAIR for processing.

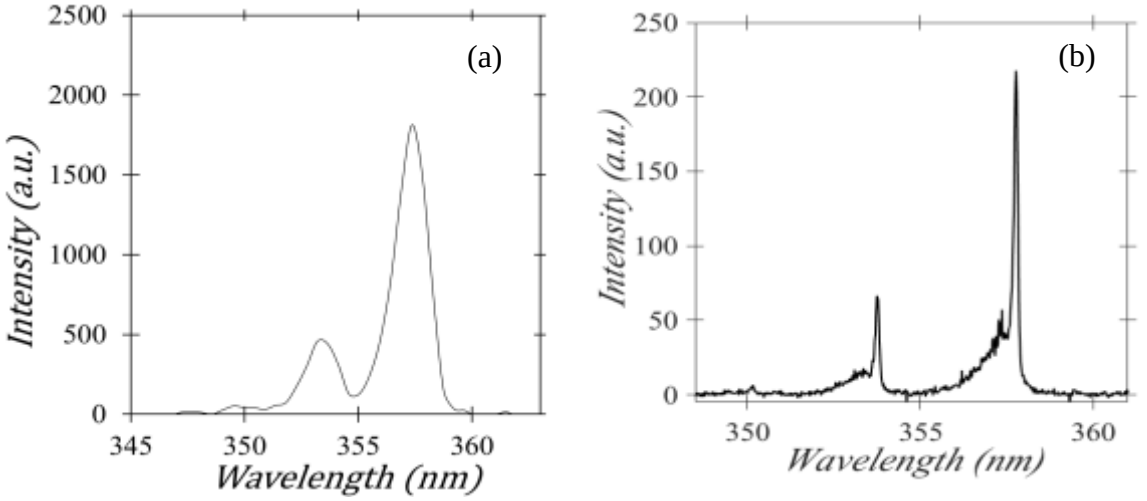

Figure 19: Comparison of (a) Helium air plasma generated at 37 kV RMS taken with the OceanOptics system in chapter 2 and (b) N_2 Second Positive system of a helium air plasma generated at 36.4 kV RMS using the 1800 g/mm grating.

Figure 19 shows that the rotational structure is more prevalent than in the previous spectra shown in chapter 2. The increased resolution and sensitivity of the Princeton Instruments system reveals much more detail than the Ocean Optics system. The spectra obtained for this voltage was very dim compared to the higher voltages, which was expected since the plasma was barely visible to the naked eye. Despite being the dimmest spectrum obtained, the signal to noise ratio of 100:1 was still sufficient to permit a SPECAIR fit. All of the spectra obtained for the N_2 Second Positive system at various voltages were taken with the same setting that produced Figure 19, to directly compare the temperatures from one voltage to the next.

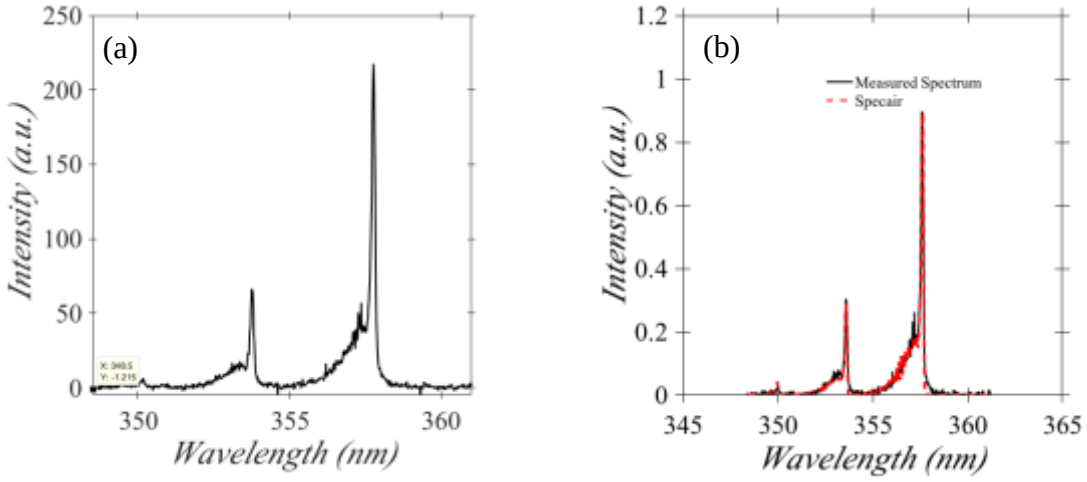

Figure 20: Helium air plasma generated at 36.4 kV RMS (a) measured spectrum and (b) is the SPECAIR fit

Figure 20 shows the SPECAIR fit for the helium air plasma generated at 36.4 kV RMS. The rotational temperature was 440 ± 100 K, vibrational temperature was 3730 ± 100 K, and the translational temperature was 468 ± 100 K. Since the rotational temperature of the N_2 Second Positive system provides a good measure of the bulk gas

temperature, this shows that the temperature is slightly above room temperature, which we attribute to the 4 min plasma run time required to achieve a good signal to noise ratio.

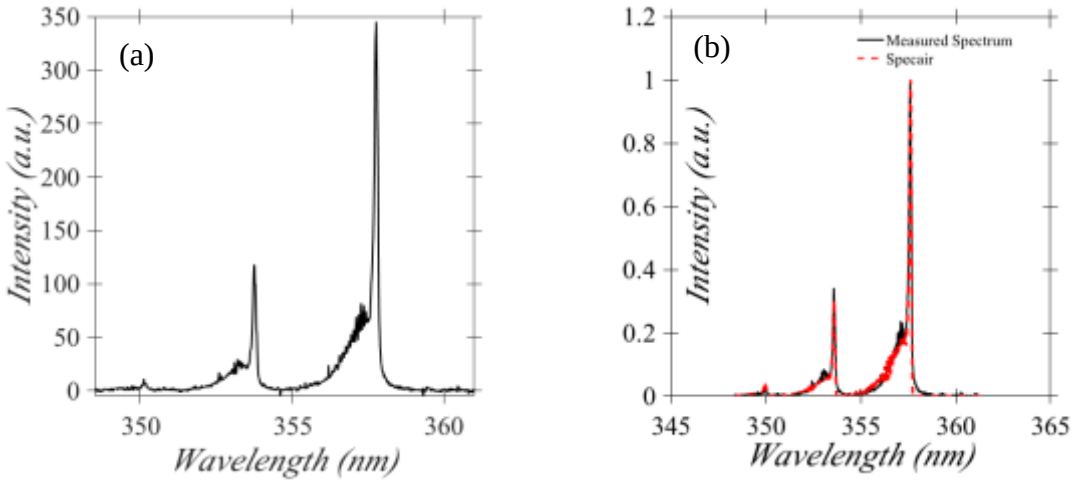

Figure 21: Helium air plasma generated at 44.8 kV RMS (a) measured spectrum and (b) is the SPECAIR fit

Figure 21 shows the SPECAIR fit for helium air plasma generated at 44.8 kV RMS. The rotational temperature was 479 ± 100 K, vibrational temperature was 3990 ± 100 K, and the translational temperature was 523 ± 100 K. These peaks are clearly more defined than those from Figure 20 since the plasma is brighter. This also makes more of the rotational structure visible in Figure 21 (a), which allows SPECAIR to obtain a more accurate fit, as shown in Figure 21 (b). The peak near 350 nm also exhibits a higher intensity, suggesting that more nitrogen is being ionized, which increases the concentration at this voltage.

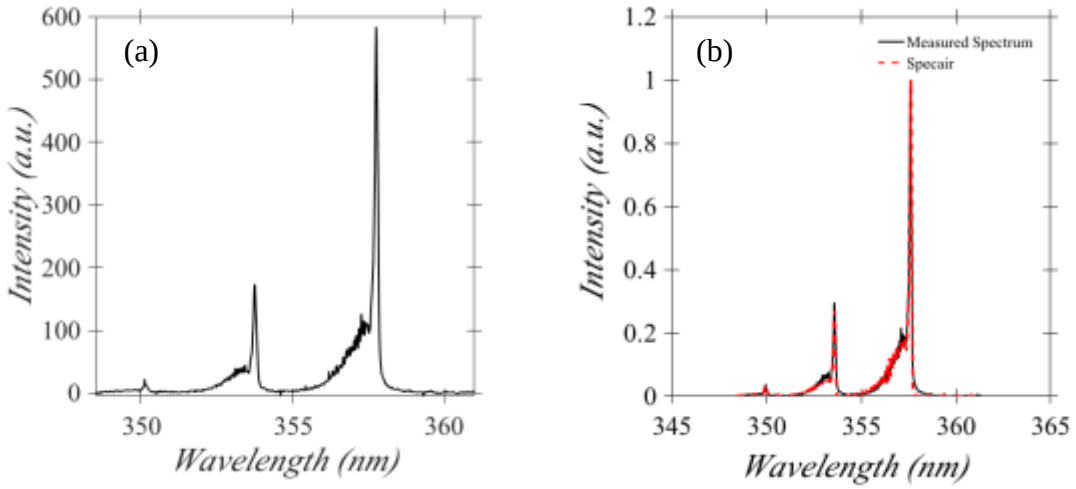

Figure 22: Helium air plasma generated at 58.1kV RMS (a) measured spectrum and (b) is the SPECAIR fit

Figure 22 shows the SPECAIR fit for helium air plasma generated at 58.1 kV RMS. The rotational temperature was 423 ± 100 K, vibrational temperature was 3441 ± 100 K, and the translational temperature was 441 ± 100 K. Again, the plasma exhibited increased intensity overall due to increased brightness, which also results in a more defined rotational structure in the spectrum. Increasing the voltage to 71.0 kV resulted in an increased intensity of the plasma as has been seen with the previous measurements. The same OES measurements were again conducted at this voltage to measure any change in temperature and speciation. Figure 23 shows the resulting spectrum as well as the SPECAIR fitting results for temperatures.

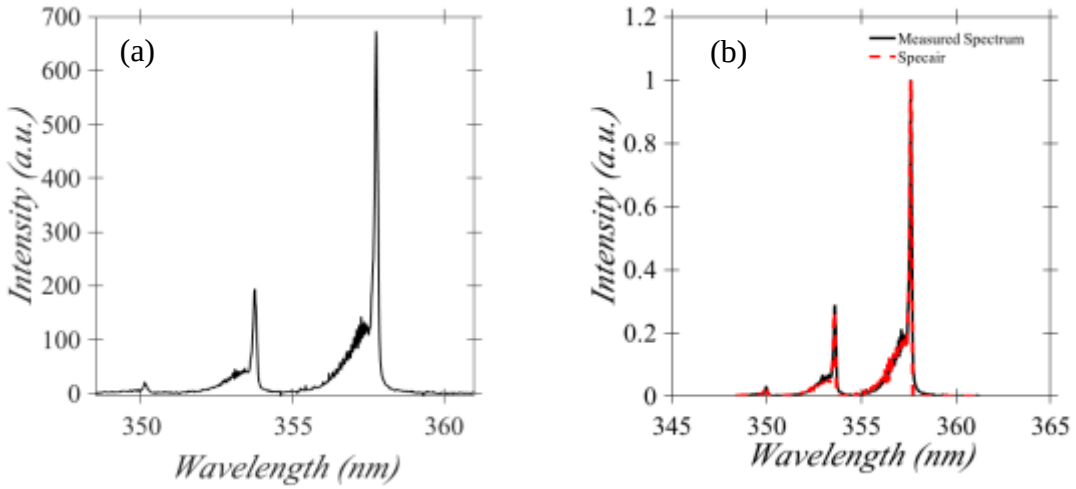

Figure 23: Helium air plasma generated at 71.0 kV RMS (a) measured spectrum and (b) is the SPECAIR fit

Figure 23 shows the SPECAIR fit for helium air plasma generated at 71.0 kV RMS. The rotational temperature was 404 ± 100 K, vibrational temperature was 3763 ± 100 K, and the translational temperature was 445 ± 100 K. The plasma generated at this voltage was the brightest and, thus, yielded the most spectral detail. The results clearly show that the increasing the voltage did not directly increase the bulk gas temperature. The rotational temperatures were 440 ± 100 K, 479 ± 100 K, 423 ± 100 K, and 404 ± 100 K for 36.4, 44.8, 58.1, and 71.0 kV RMS applied, respectively. Table 5 reports the plasma temperatures for each voltage setting.

Table 5: The rotational temperature (T_R), vibrational temperature (T_v), electronic temperature (T_e), and the translational temperature (T_T) for a Helium air plasma are reported with ± 100 K error.

Voltage (kV)	T_T	T_e	T_V	T_R
36.4	468	10000	3730	440
44.8	523	10000	3990	479
58.1	441	10000	3441	423
71.0	445	10000	3736	404

The next measurement was obtained to better understand how the increased power affects the plasma since temperature does not necessarily increase. The "Step and Glue" function of the spectrometer was utilized to observe any change in the species generated in the plasma over the 250 to 500 nm wavelength range. This function starts at 250 nm and goes to 500 nm in sections of approximately 10 nm and stitches them together to form a larger wavelength range. Figure 24 shows a representative spectrum of the "Step and Glue" process.

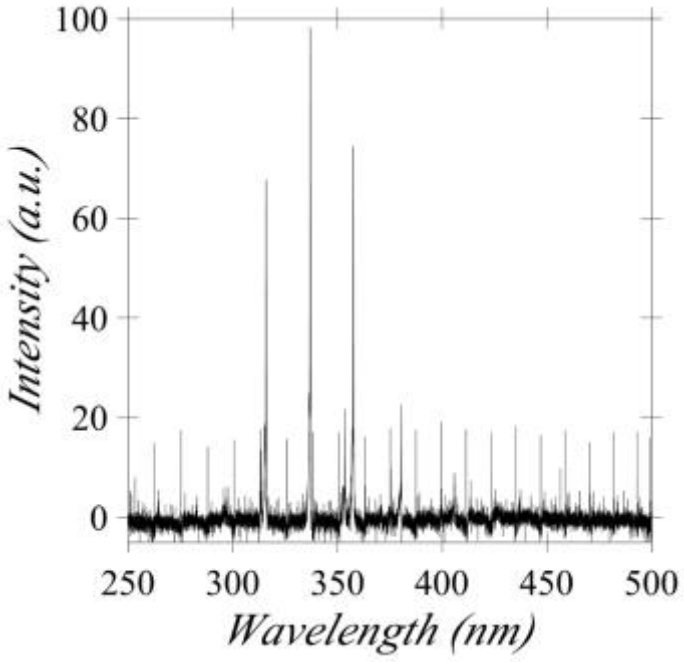

Figure 24: Spectrum ranging from 250 to 500 nm for a helium air plasma generated using 36.4 kV RMS with high noise. The N_2 second positive system can still be seen in detail.

Figure 3.7 shows the "Step and Glue" spectrum ranging from 250 to 500 nm with high noise observed in the signal. Periodic spikes arise with roughly equal intensity across the entire spectrum. The noise is due to the large gain required by intensifier to obtain a signal from the very dim diffuse discharge. The movement of the grating to

obtain a larger wavelength range also creates noise when the sections are glued together. The noise spikes occur at the locations of the "gluing" process of the multiple spectra taken. The N_2 Second Positive system, from 300 to 400 nm, is still seen in detail although surrounded by noise. While this spectrum provides no real information for 36.4 kV RMS, higher voltage settings produced more favorable spectra.

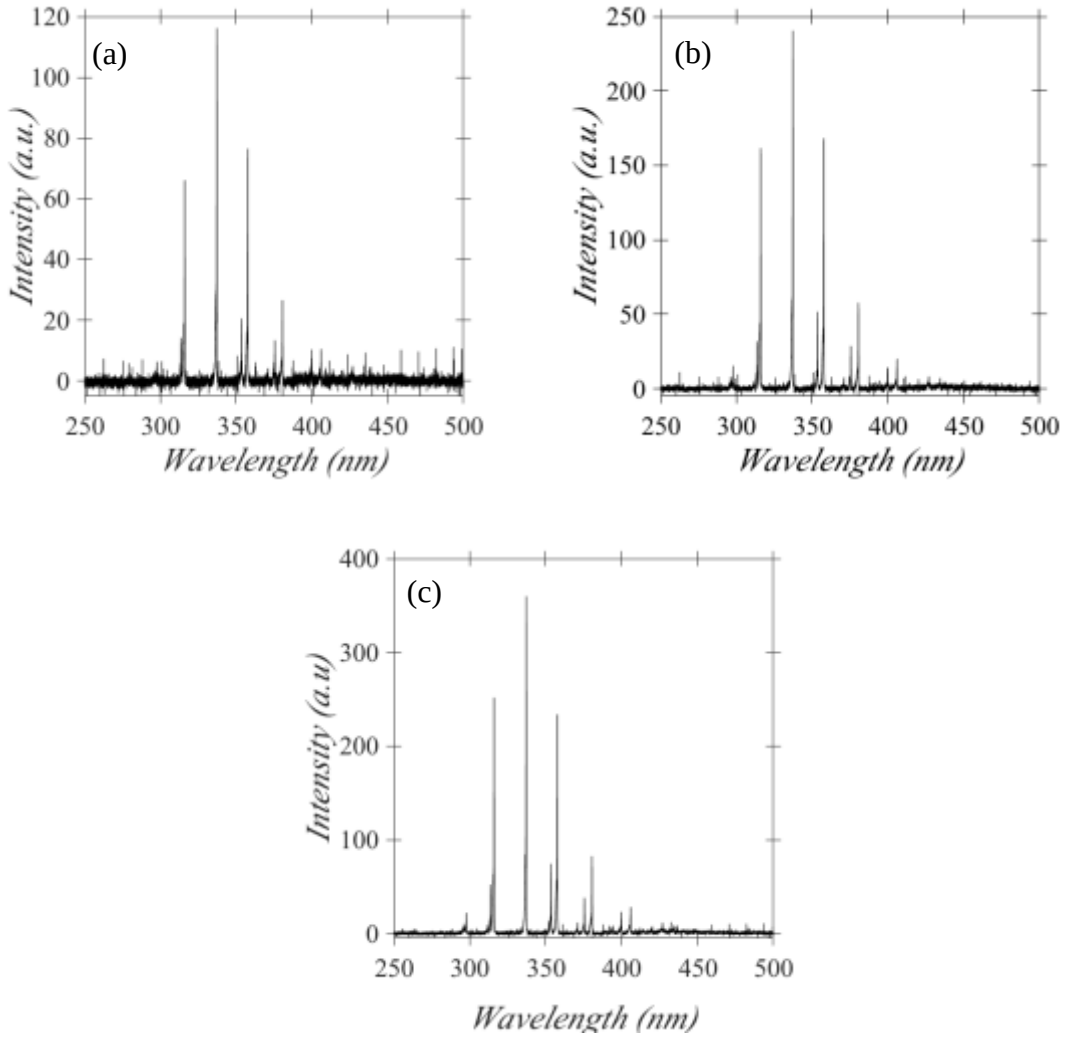

Figure 25: "Step and Glue" spectra showing 250 to 500 nm for a helium air plasma generated at a) 44.8 RMS, (b) 58.1 kV RMS, and (c) 71.0 kV RMS.

Figure 25 shows the "Step and Glue" spectrum ranging from 250 to 500 nm for 44.8 kV RMS, 58.1 kV RMS, and 71.0 kV RMS. Increasing the voltage changed the species observed in the plasma with more of the N_2 Second Positive system observed higher relative intensities. Table 6 shows the observed species in plasmas generated by (a) 36.4 kV RMS, (b) 44.8 kV RMS, (c) 58.1 kV RMS, and (d) 71.0 kV RMS. For the 36.4 and 44.8 kV RMS plasmas, only N_2 and N_2^+ are observed in the 250 to 500 nm range. For the plasmas generated at 58.1 and 71.0 kV RMS N_2, N_2^+, and OH are observed. This shows that increasing the system voltage impacts the species production rather than increasing the temperature. The relative intensities have been plotted in Figure 26 to show the change in relative intensity and therefore concentration.

Table 6: Species observed in plasma generated by (a) 36.4 kV RMS, (b) 44.8 kV RMS, (c) 58.1 kV RMS, (d) 71.0 kV RMS applied to the helium air mixture.

Wavelength	Species	Plasma which species were observed
295.12	OH	d
296.24	OH	c,d
315.93	N_2	a,b,c,d
337.13	N_2	a,b,c,d
353.67	N_2	b,c,d
357.69	N_2	a,b,c,d
375.54	N_2	b,c,d
380.49	N_2	b,c,d
399.84	N_2	b,c,d
405.94	N_2	b,,c,d
427.81	N^+_2	b,c,d

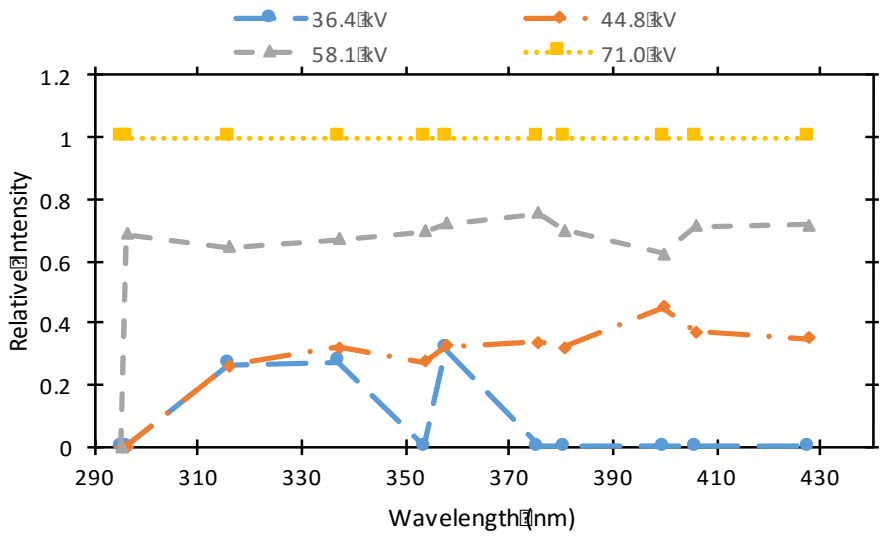

Figure 26: Relative intensities of the peaks in Table 6 showing the intensity of the peaks and thus concentration, increased with higher voltage.

Figure 26 shows that the change in the relative intensity of all the peaks corresponds to changes in voltage, suggesting that higher voltages lead to more species production for N_2, N_2^+, and OH reactive species. This may potentially mean that shorter treatment times can be used to treat samples, which could potentially reduce any thermal effects that could arise due to extended time periods in field. It should be noted that the absence of peaks in the 36.4 kV plasma does not mean that the species were not present. The ICCD and spectrometer system have noise associated with each measurement that limits the lowest peak detectable. Therefore, the absence of peaks most likely implies that the species were just too dim to be detected by our system. The combination of ICCD sensitivity, gain setting of the intensifier, and light lost during collection could make the weaker peaks indistinguishable from this noise.

The voltage applied was measured to ensure that all parameters were accounted for and that the applied voltage was accurately presented. Figure 27 shows voltage waveforms that would be expected of a DDB type discharge for an applied voltage of 36.4 kV RMS. Noise is observed on the waveform as can be seen by the voltage spikes that are in Figure 27.

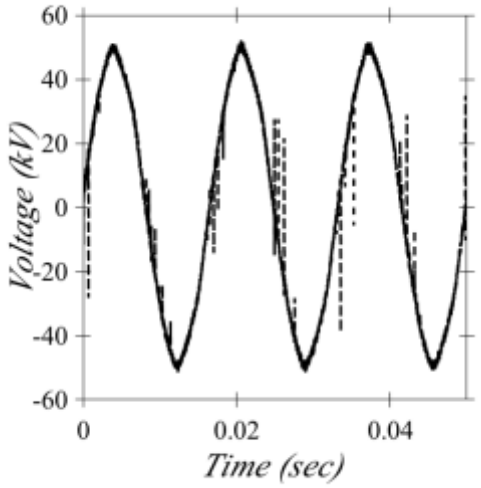

Figure 27: Voltage and current waveform for 36.4 kV RMS showing DBD type current spikes.

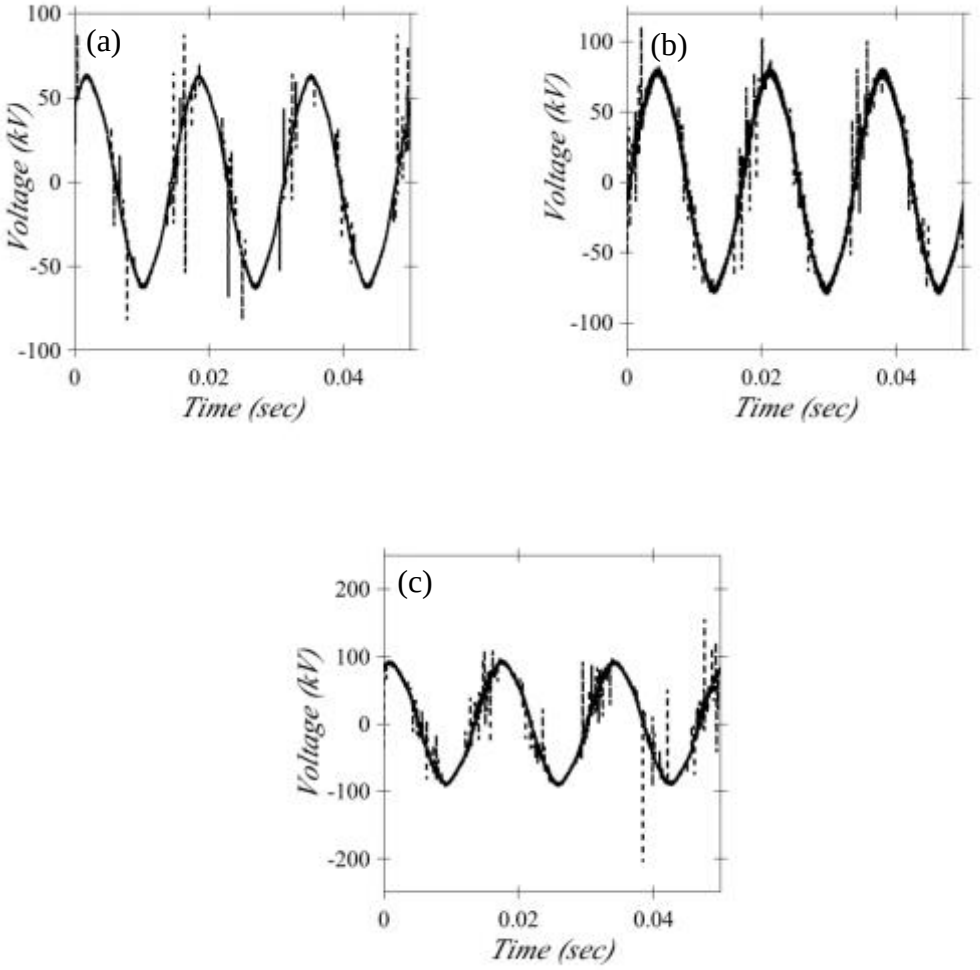

Figure 28: Voltage and current waveforms for a helium air plasma generated at a) 44.8 kV RMS, (b) 58.1 kV RMS, and (c) 71.0 kV RMS.

Figure 28 shows the waveforms for the voltage measurement for the applied 44.8, 58.1, and 71.0 kV RMS. The noise appears to increase with the higher applied voltage, as shown in part (c) of Figure 28. We hypothesize that this arises because of the induced voltage caused by the high electric fields generated by the system. Improperly shielded electronics and materials can pick up charge and malfunction. Even when shielded, we observed noise in most cases, although the noise observed here is sufficiently low to not

skew the measurement of the applied voltage. Therefore, we could accurately capture the voltage applied to the system for all OES measurements.

CHAPTER 4. CONCLUSION

This thesis elucidated how plasma properties, particularly species generation, voltage, and current, varied with container material and applied voltage. HVCAPs offer a safe, cost effective treatment method for food products. Previous work characterized the bactericidal effects of HVCAPs to demonstrate their viability as an alternative to many costly and potentially toxic methods currently used in industry [27,29]. Most prior work focused on sterilization efficacy and treatment time [17,28], which left a gap in understanding how the plasma itself and container material influenced the measurement and treatment processes. The current work specifically explored how packaging and fill gas altered OES measurements and various plasma temperature parameters.

OES measurements showed that the container material decreased the intensity by 61.9% 63.2%, and 64.2% with a standard deviation of 0.94% while the bag decreased intensity for each peak by between 44.2% and 45.4% with a standard deviation of 0.49% with no change in the species composition of the plasma. This suggests that the choice of material to seal the container may not influence the chemistry of the process. Further analysis utilizing a higher resolution spectrometer will better elucidate this phenomenon.

We further observed that the rotational temperatures ranged from 1088 K ± 100 for nitrogen to 1421 ± 100 K for compressed air while rotational temperatures ranged from 479 ± 100 K for helium to 285 ± 100 K for compressed air. This differs from values obtained in previous work conducted at 15 kV, showing the translational temperature to be 300 ± 100 K [28]. Lissajous diagrams showed that the power dissipated by the nitrogen and ambient air plasmas were comparable to the compressed dry air discharge while helium discharges absorbed approximately 92% more power.

The species and power measurements indicate that an ambient air plasma induces similar species at similar or lower power dissipations than other gases used in this study. This suggests that it may be more economical to forgo purchasing other fill gases and simply treat food product in ambient air. However, this study only explores a small number of voltage parameters and does not provide a comprehensive analysis of all species generated. Further investigation with a higher resolution spectrometer will more fully assess the species generated, particularly those that may arise in low concentrations, and enable studies into their importance for sterilization. Ultimately, tuning species generation to bactericidal efficacy while retaining food quality require both microbiology experiments and a better understanding of the fundamental biophysical phenomena. Although effective, practical applications of CAPs for treating sealed food packages require elucidating the impact of the packaging material to optimize treatment efficacy and verifying the absence of potential hazardous molecules and species from the package [70]. This is particularly important since plasmas are well known for modifying surface and material properties. For instance, a 12kV DBD increased the OH concentration on a

glass surface for etching [58]. Thus, potential industrial applications would motivate the selection of materials more resistant to chemical breakdown to prevent the release of potentially hazardous molecules. Combining these efforts with an enhanced understanding of the fundamental biophysical phenomena [71,72] will allow us to understand how the species created induce the desired effect and how to design appropriate systems to create these species for system optimization.

We next assessed the effect of voltage on species generation using a helium air plasma generated using the Phenix system with applied voltages of 36.4, 44.8, 58.1, and 71.0 kV. The light from the plasma was collected using a fiber optic cable that was provided with the SP2500 spectrometer. We simultaneously measured electrical and OES data and processed it using custom MATLAB scripts to plot the current and voltage, N_2 Second Positive system, spectra ranging from 250 to 500 nm to observe species generation, and text files that were fed into SEPCAIR to calculate temperatures.

The N_2 Second Positive system of a helium air plasma generated at 36.4 kV was observed using the 1800 g/mm grating of a spectrometer. The spectra obtained for this voltage was very dim compared to the higher voltages, which was expected since the plasma was barely visible to the naked eye. SPECAIR fits for the spectra are summarized in Table 5 and show no real correlation to voltage. Higher voltage did not necessarily translate to higher plasma temperature. This suggests that it is possible to optimize a high voltage system to obtain reactive species while maintaining low temperatures.

We next evaluated the species generated during the plasma treatment. The relative intensities for the observed peaks for each voltage were plotted and shown to increase with a corresponding increase in voltage. It was clearly seen that the increased voltage did not directly correlate to increased temperature of the bulk gas as presented in Table 5. For the 36.4 and 44.8 kV plasma, only N_2 and N_2^+ are observed in the 250 to 500 nm range. For the plasmas generated at 58.1 and 71.0 kV N_2, N_2^+, and OH are observed as shown in Table 6 for each voltage setting. This showed that increasing system voltage/power produced higher species concentrations rather than increasing the temperature.

The voltage was recorded for each data run to ensure that every parameter was accounted for in the evaluation of the plasma properties. Figures 27 and 28 show the measured waveforms for each of the OES data runs. Although noise existed for each case, it did not skew the measured voltage. It was seen that the noise increased for the higher voltage settings as would be expected from our system. High levels of noise are commonly induced due to the high electric fields the systems creates, routinely interrupting electronics in the room. This was accounted for and shielded to the best of our ability and did not affect the data collected. It was observed that the plasma voltages were 36.4, 44.8, 58.1, and 71.0 kV RMS for the respective OES runs. This covered the entire range that is sustained by the system at this time.

This work has shown the potential of CAPs to treat products at low temperatures and still be able to produce reactive species. It is now clear that a parameter space can be

explored to optimize the treatment process without concern for the effects of the container material used to hold the working gas and product. It was also shown that higher voltages generate higher concentrations of radical species while not directly correlating to an increase in intensity. The higher voltages also appeared to have minimal effect on the container material, as no change in speciation was observed in the wavelength range chosen for the study. Still, future studies for HVCAPs must address species generation at higher voltages in different wavelength ranges and with different gases. The spectroscopy system used in these experiments was extremely sensitive to the 200-500 nm range, which provides some detail about the plasma properties and species. Light above that range was too dim for our system to distinguish with the settings used. Better understanding radical species generation requires expanding the setup and optimizing the analysis to better characterize wavelengths above 500 nm. The high voltage settings for this system have only been explored as a function of voltage for helium air mixtures. The food industry uses numerous gas blends that must also be explored for safety and reliability. This will provide a detailed parameter space that can be used to industrialize this technology.

LIST OF REFERENCES

LIST OF REFERENCES

[1] Kanazawa S, Kogoma M, Moriwaki T and Okazaki S 1988 Stable glow plasma at atmospheric pressure *J. Phys. D. Appl. Phys.* **21** 838–40

[2] Bárdos L and Baránková H 2010 Cold atmospheric plasma: Sources, processes, and applications *Thin Solid Films* **518** 6705–13

[3] Fauchais P and Vardelle A 1997 Thermal plasmas *IEEE Trans. Plasma Sci.* **25** 1258–80

[4] Teulet P, Girard L, Razafinimanana M, Gleizes a, Bertrand P, Camy-Peyret F, Baillot E and Richard F 2006 Experimental study of an oxygen plasma cutting torch: II. Arc–material interaction, energy transfer and anode attachment *J. Phys. D. Appl. Phys.* **39** 1557–73

[5] Freton P, Gonzalez J J, Gleizes a, Peyret F C, Caillibotte G and Delzenne M 2001 Numerical and experimental study of a plasma cutting torch *J. Phys. D. Appl. Phys.* **35** 115–31

[6] Matsumoto S, Hino M and Kobayashi T 1987 Synthesis of diamond films in a rf induction thermal plasma *Appl. Phys. Lett.* **51** 737–9

[7] Chu P K and Lu X 2013 *Low Temperature Plasma Technology Methods and Applications.* (CRC Press (an imprint of Taylor & Francis))

[8] Chen F F 1995 Industrial applications of low-temperature plasma physics *Phys. Plasmas* **2** 2164

[9] Laroussi M and Akan T 2007 Arc-free atmospheric pressure cold plasma jets: A review *Plasma Process. Polym.* **4** 777–88

[10] Stoffels E 2007 "Tissue Processing" with Atmospheric Plasmas *Contrib. to Plasma Phys.* **47** 40–8

[11] Kogelschatz U 2003 Dielectric-barrier discharges: their history, discharge physics, and industrial applications *Plasma Chem. Plasma Process.* **23** 1–46

[12] Conrads H and Schmidt M 2000 Plasma generation and plasma\rsources *Plasma Sources Sci. Technol.* **9** 441–54

[13] Motret O, Hibert C, Pellerin S and Pouvesle J M 2000 Rotational temperature measurements in atmospheric pulsed dielectric barrier discharge - gas temperature and molecular fraction effects *J. Phys. D. Appl. Phys.* **33** 1493–8

[14] Ware W R 1971 Nanosecond Time-Resolved Emission Spectroscopy: Spectral Shifts due to Solvent-Excited Solute Relaxation *J. Chem. Phys.* **54** 4729

[15] Chen J and Wang P 2005 Effect of relative humidity on electron distribution and ozone production by DC coronas in air *IEEE Trans. Plasma Sci.* **33** 808–12

[16] Preis S, Klauson D and Gregor a. 2013 Potential of electric discharge plasma methods in abatement of volatile organic compounds originating from the food industry *J. Environ. Manage.* **114** 125–38

[17] Klockow P A and Keener K M 2009 Safety and quality assessment of packaged spinach treated with a novel ozone-generation system *LWT - Food Sci. Technol.* **42** 1047–53

[18] Patil S, Moiseev T, Misra N N, Cullen P J, Mosnier J P, Keener K M and Bourke P 2014 Influence of high voltage atmospheric cold plasma process parameters and role of relative humidity on inactivation of Bacillus atrophaeus spores inside a sealed package *J. Hosp. Infect.* **88** 162–9

[19] Miao H and Yun G 2011 The sterilization of Escherichia coli by dielectric-barrier discharge plasma at atmospheric pressure *Appl. Surf. Sci.* **257** 7065–70

[20] Hayashi N, Guan W, Tsutsui S, Tomari T and Hanada Y 2006 Sterilization of medical equipment using radicals produced by oxygen/water vapor RF plasma *Japanese J. Appl. Physics, Part 1 Regul. Pap. Short Notes Rev. Pap.* **45** 8358–63

[21] Isbary G, Heinlin J, Shimizu T, Zimmermann J L, Morfill G, Schmidt H U, Monetti R, Steffes B, Bunk W, Li Y, Klaempfl T, Karrer S, Landthaler M and Stolz W 2012 Successful and safe use of 2 min cold atmospheric argon plasma in chronic wounds: Results of a randomized controlled trial *Br. J. Dermatol.* **167** 404–10

[22] Suhem K, Matan N, Nisoa M and Matan N 2013 Inhibition of Aspergillus flavus on agar media and brown rice cereal bars using cold atmospheric plasma treatment *Int. J. Food Microbiol.* **161** 107–11

[23] Kong M G, Kroesen G, Morfill G, Nosenko T, Shimizu T, van Dijk J and Zimmermann J L 2009 Plasma medicine: an introductory review *New J. Phys.* **11** 115012

[24] Kuchenbecker M, Bibinov N, Kaemlimg a, Wandke D, Awakowicz P and Viöl W 2009 Characterization of DBD plasma source for biomedical applications *J. Phys. D. Appl. Phys.* **42** 45212

[25] O'Connor N, Cahill O, Daniels S, Galvin S and Humphreys H 2014 Cold atmospheric pressure plasma and decontamination. Can it contribute to preventing hospital-acquired infections? *J. Hosp. Infect.* **88** 59–65

[26] Vujošević D, Mozetič M, Cvelbar U, Krstulović N and Milošević S 2007 Optical emission spectroscopy characterization of oxygen plasma during degradation of Escherichia coli *J. Appl. Phys.* **101** 103305

[27] Trinetta V, Vaidya N, Linton R and Morgan M 2011 A comparative study on the effectiveness of chlorine dioxide gas, ozone gas and e-beam irradiation treatments for inactivation of pathogens inoculated onto tomato, cantaloupe and lettuce seeds *Int. J. Food Microbiol.* **146** 203–6

[28] Connolly J, Valdramidis V P, Byrne E, Karatzas K A, Cullen P J, Keener K M and Mosnier J P 2013 Characterization and antimicrobial efficacy against E. coli of a helium/air plasma at atmospheric pressure created in a plastic package *J. Phys. D. Appl. Phys.* **46** 35401

[29] Andrews L S, Key A M, Martin R L, Grodner R and Park D L 2002 Chlorine dioxide wash of shrimp and crawfish an alternative to aqueous chlorine *Food Microbiol.* **19** 261–7

[30] Laroussi M 2009 Low-temperature plasmas for medicine? *IEEE Trans. Plasma Sci.* **37** 714–25

[31] Fridman G, Shereshevsky A, Jost M M, Brooks A D, Fridman A, Gutsol A, Vasilets V and Friedman G 2007 Floating electrode dielectric barrier discharge plasma in air promoting apoptotic behavior in Melanoma skin cancer cell lines *Plasma Chem. Plasma Process.* **27** 163–76

[32] Fridman A, Chirokov A and Gutsol A 2005 Non-thermal atmospheric pressure discharges *J. Phys. D* **38** R21–4

[33] Chiper A S, Chen W, Mejlholm O, Dalgaard P and Stamate E 2011 Atmospheric pressure plasma produced inside a closed package by a dielectric barrier discharge in Ar/CO2 for Bacterial Inactivation of Biological Samples *Plasma Sources Sci. Technol.* **20** 25008

[34] Chiper A S and Popa G 2011 Temporal and spatial resolved emission spectroscopy of a pulsed atmospheric-pressure DBD in helium with impurities *IEEE Trans. Plasma Sci.* **39** 2196–7

[35] Moiseev T, Misra N N, Patil S, Cullen P J, Bourke P, Keener K M and Mosnier J P 2014 Post-discharge gas composition of a large-gap DBD in humid air by UV–Vis absorption spectroscopy *Plasma Sources Sci. Technol.* **23** 65033

[36] Panousis E, Ricard A, Loiseau J-F, Clément F and Held B 2009 Estimation of densities of active species in an atmospheric pressure N2 DBD flowing afterglow using optical emission spectroscopy and analytical calculations *J. Phys. D. Appl. Phys.* **42** 205201

[37] Bashir M, Rees J M and Zimmerman W B 2013 Plasma polymerization in a microcapillary using an atmospheric pressure dielectric barrier discharge *Surf. Coatings Technol.* **234** 82–91

[38] Schutze A, Jeong J Y, Babayan S E, Park J, Selwyn G S and Hicks R F 1998 The atmospheric-pressure plasma jet: a review and comparison to other plasma sources *Plasma Sci. IEEE Trans.* **26** 1685–94

[39] Akamatsu H and Ichikawa K 2011 Characteristics of atmospheric pressure plasma jet generated by compact and inexpensive high voltage modulator *Surf. Coatings Technol.* **206** 920–4

[40] Deng X L, Nikiforov A Y, Vanraes P and Leys C 2013 Direct current plasma jet at atmospheric pressure operating in nitrogen and air *J. Appl. Phys.* **113**

[41] Wattieaux G, Yousfi M and Merbahi N 2013 Optical emission spectroscopy for quantification of ultraviolet radiations and biocide active species in microwave argon plasma jet at atmospheric pressure *Spectrochim. Acta - Part B At. Spectrosc.* **89** 66–76

[42] Xiong Q, Nikiforov A Y, González M Á, Leys C and Lu X P 2013 Characterization of an atmospheric helium plasma jet by relative and absolute optical emission spectroscopy *Plasma Sources Sci. Technol.* **22** 15011

[43] Fröhling A, Durek J, Schnabel U, Ehlbeck J, Bolling J and Schlüter O 2012 Indirect plasma treatment of fresh pork : Decontamination ef fi ciency and effects on quality attributes *Innov. Food Sci. Emerg. Technol.* **16** 381–90

[44] Isbary G, Morfill G, Schmidt H U, Georgi M, Ramrath K, Heinlin J, Karrer S, Landthaler M, Shimizu T, Steffes B, Bunk W, Monetti R, Zimmermann J L, Pompl R and Stolz W 2010 A first prospective randomized controlled trial to decrease bacterial load using cold atmospheric argon plasma on chronic wounds in patients *Br. J. Dermatol.* **163** 78–82

[45] Li J, Zhu X and Pu Y 2011 A novel method of using the OES line ratio to determine the spatially resolved atomic density in low-temperature plasmas and its application in carbon and aluminium atoms in capacitively coupled plasmas *J. Phys. D. Appl. Phys.* **44** 455203

[46] Zhu X and Pu Y 2008 Using OES to determine electron temperature and density in low-pressure nitrogen and argon plasmas *Plasma Sources Sci. Technol. Plasma Sources Sci. Technol* **17** 24002–6

[47] Stancu G D, Kaddouri F, Lacoste D A and Laux C O Atmospheric pressure plasma diagnostics by OES , CRDS and TALIF **124002**

[48] Aragón C and Aguilera J A 2008 Characterization of laser induced plasmas by optical emission spectroscopy: A review of experiments and methods *Spectrochim. Acta Part B At. Spectrosc.* **63** 893–916

[49] Zimmer L and Tachibana S 2007 Laser induced plasma spectroscopy for local equivalence ratio measurements in an oscillating combustion environment *Proc. Combust. Inst.* **31 I** 737–45

[50] Fantz U 2006 Basics of plasma spectroscopy **15**

[51] Donnelly V M 2004 Plasma electron temperatures and electron energy distributions measured by trace rare gases optical emission spectroscopy *J. Phys. D. Appl. Phys.* **37** R217–36

[52] Coburn J W and Chen M 1980 Optical emission spectroscopy of reactive plasmas: A method for correlating emission intensities to reactive particle density *J. Appl. Phys.* **51** 3134

[53] Förster S, Mohr C and Viöl W 2005 Investigations of an atmospheric pressure plasma jet by optical emission spectroscopy *Surf. Coatings Technol.* **200** 827–30

[54] Bruggeman P, Verreycken T, González M Á, Walsh J L, Kong M G, Leys C and Schram D C 2010 Optical emission spectroscopy as a diagnostic for plasmas in liquids: opportunities and pitfalls *J. Phys. D. Appl. Phys.* **43** 124005

[55] Sarani A, Nikiforov A Y and Leys C 2010 Atmospheric pressure plasma jet in Ar and Ar/H2O mixtures: Optical emission spectroscopy and temperature measurements *Phys. Plasmas* **17** 63504

[56] Xiong Q, Lu X P, Ostrikov K, Xian Y, Zou C, Xiong Z and Pan Y 2010 Pulsed dc- and sine-wave-excited cold atmospheric plasma plumes: A comparative analysis *Phys. Plasmas* **17** 43506

[57] Bruggeman P, Schram D, González M Á, Rego R, Kong M G and Leys C 2009 Characterization of a direct dc-excited discharge in water by optical emission spectroscopy *Plasma Sources Sci. Technol.* **18** 25017

[58] Wang C, Zhang G, Wang X and He X 2010 The effect of air plasma on barrier dielectric surface in dielectric barrier discharge *Appl. Surf. Sci.* **257** 1698–702

[59] Švorčík V, Kotál V, Slepička P, Bláhová O, Špírková M, Sajdl P and Hnatowicz V 2006 Modification of surface properties of polyethylene by Ar plasma discharge *Nucl. Instruments Methods Phys. Res. Sect. B Beam Interact. with Mater. Atoms* **244** 365–72

[60] McKeen L W and Plastics Design Library. 2013 *The effect of UV light and weather on plastics and elastomers* (William Andrew)

[61] Biganzoli I, Barni R, Gurioli A, Pertile R and Riccardi C 2014 Experimental investigation of Lissajous figure shapes in planar and surface dielectric barBiganzoli, I., Barni, R., Gurioli, a, Pertile, R., & Riccardi, C. (2014). Experimental investigation of Lissajous figure shapes in planar and surface dielectric barr *J. Phys. Conf. Ser.* **550** 12039

[62] Winter J, Wende K, Masur K, Iseni S, Dünnbier M, Hammer M U, And H T, Weltmann K-D and Reuter S 2013 Feed gas humidity: a vital parameter affecting a cold atmospheric-pressure plasma jet and plasma-treated human skin cells *J. Phys. D. Appl. Phys.* **46**295401 (11pp)

[63] Pearse R W B (Reginald W B 1976 *The identification of molecular spectra* ed A G (Alfred G Gaydon (London : New York: London : Chapman and Hall)

[64] NIST Atomic Data for Nitrogen (N)

[65] NIST Atomic Data for Helium (He)

[66] Wagner H, Brandenburg R, Kozlov K V, Sonnenfeld A and Michel P 2003 The barrier discharge : basic properties and applications to surface treatment *Vacuum* **71** 417–36

[67] Kogelschatz U, Eliasson B and Egli W 1997 Dielectric-Barrier Discharges. Principle and Applications *J. Phys. IV Colloq.* **4** 7–4

[68] Zhang C, Shao T, Yu Y, Niu Z, Yan P and Zhou Y 2010 Comparison of experiment and simulation on dielectric barrier discharge driven by 50 Hz AC power in atmospheric air *J. Electrostat.* **68** 445–52

[69] Kogelschatz U 2003 Dielectric-barrier Discharges : Their History , Discharge Physics , and Industrial Applications **23** 1–46

[70] Fang Z, Wang X, Shao R, Qiu Y and Edmund K 2011 The effect of discharge power density on polyethylene terephthalate film surface modification by dielectric barrier discharge in atmospheric air *J. Electrostat.* **69** 60–6

[71] Graves D B 2012 The emerging role of reactive oxygen and nitrogen species in redox biology and some implications for plasma applications to medicine and biology *J. Phys. D Appl. Phys.* **45** 263001–42

[72] Babaeva N Y, Tian W and Kushner M J 2014 The interaction between plasma filaments in dielectric barrier discharges and liquid covered wounds: electric fields delivered to model platelets and cells *J. Phys. D. Appl. Phys.* **47** 1–11

APPENDICES

Appendix A

SPECAIR is a software program from Spectral Fit in Antony, France that uses discharge models to calculate a spectrum, and then fits that synthetic spectrum to measured data. This Appendix will describe the process used to obtain spectral fits and temperatures.

Figure 29 shows the initial screen that the user encounters upon opening the software.

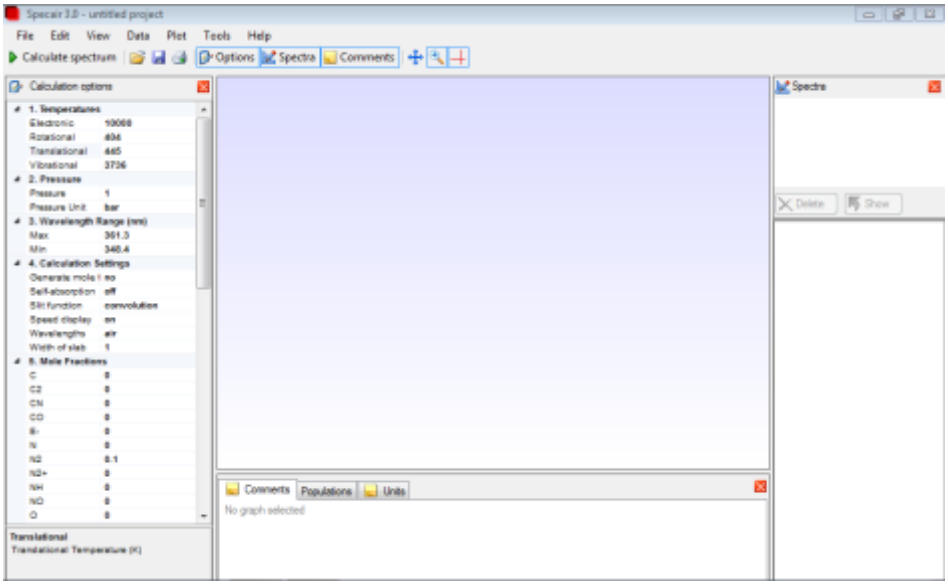

Figure 29: Initial Screen presented to user when opening SPECAIR.

From this screen, the user can access all the needed tools to find temperatures. The left-hand window displays the calculation options that may either be entered by the user or obtained from the software by fitting to measured spectra. The center blue screen will display the selected spectra that are displayed on the right in the “spectra” section. The white area below the “spectra” section will display the relevant properties of the selected

spectra. To analyze the data, the user will first verify the slit function. This requires clicking on the “Tools” dropdown menu and selecting “Slit function” as shown in Figure 30.

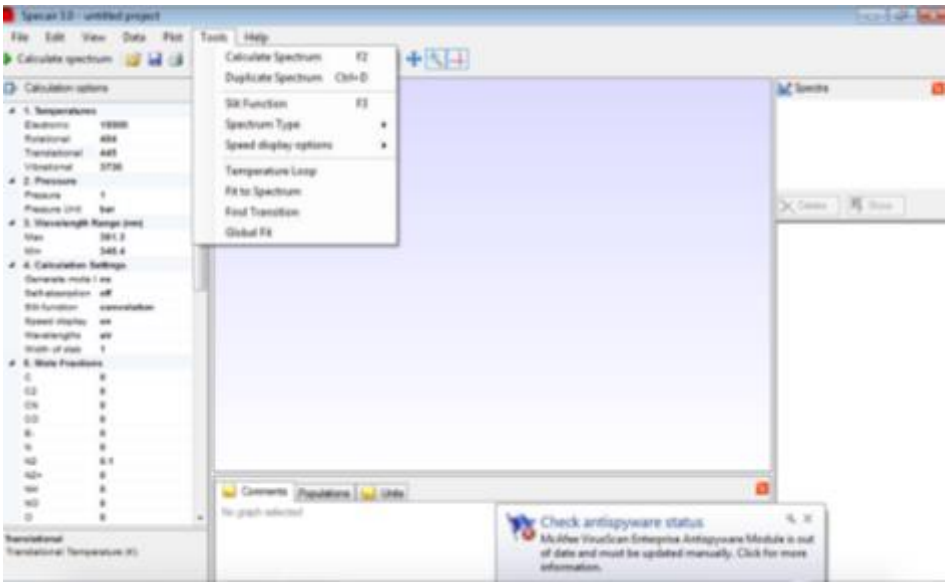

Figure 30: Tools drop down menu for altering calculation options and modifying slit function.

This subsequently displays a new screen shown in Figure 31 that allows the user to modify the slit function. The user may import a measured slit function or specify an estimated function in the window shown in Figure 31. The SPECAIR manual provides a detailed explanation of the slit function and methods for estimating it.

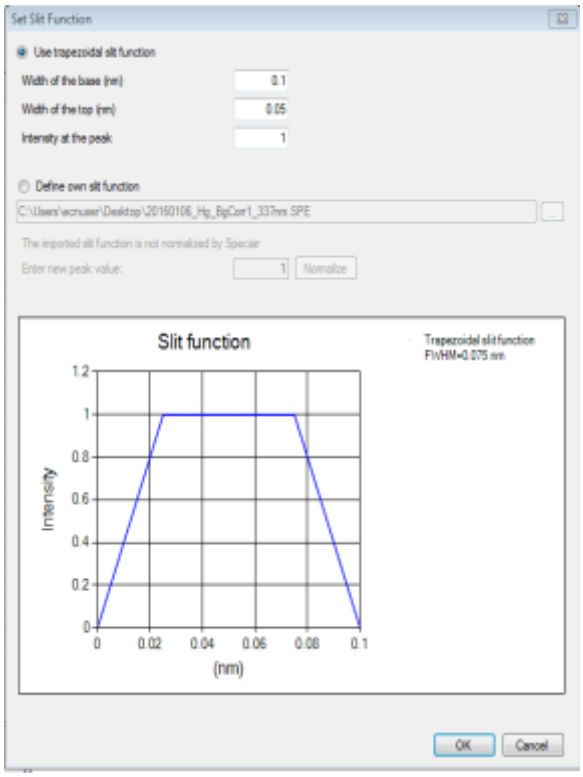

Figure 31: Slit function settings menu allowing for user entered parameters or importing measured functions.

Next, the user goes to the "File" tab of the top drop down menus and imports the measured spectrum. The software can recognize certain formats, such as SPE files, so I always convert mine to text file consisting of two columns giving wavelength and intensity, which works well. Figure 32 shows the spectrum displayed in the center screen following successful importing.

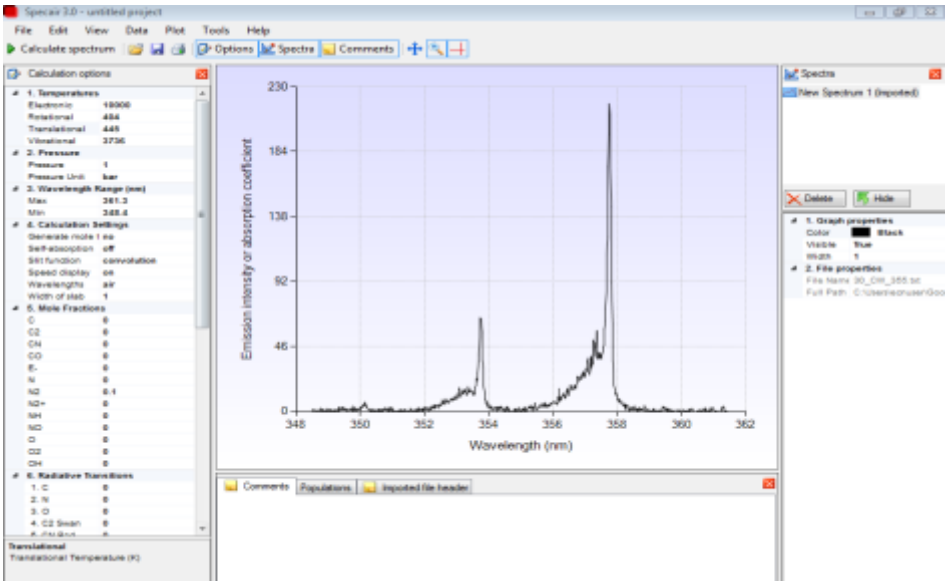

Figure 32: Imported spectrum displayed in center window of SPECAIR ready to undergo fitting.

The user may then identify transitions and start the fitting process. The user should ensure that the imported spectrum is selected in the window on the right, as shown in Figure 33, since other spectra will appear in this window during the fitting process.

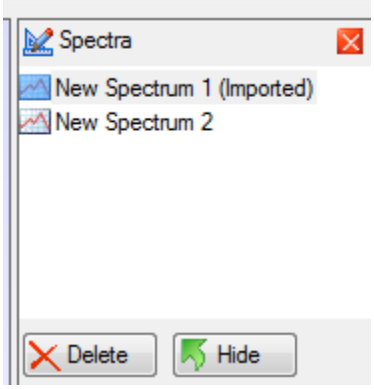

Figure 33: Properly selected spectra to conduct transition identification and fitting.

Once selected the next step is to go into the “Tools” menu and select “Find Transition”, which identifies the transitions in SPECAIR’s database present in the spectrum and

available to be fit via the synthetic spectrum. Figure A.6 illustrates the window that pops up to identify transitions.

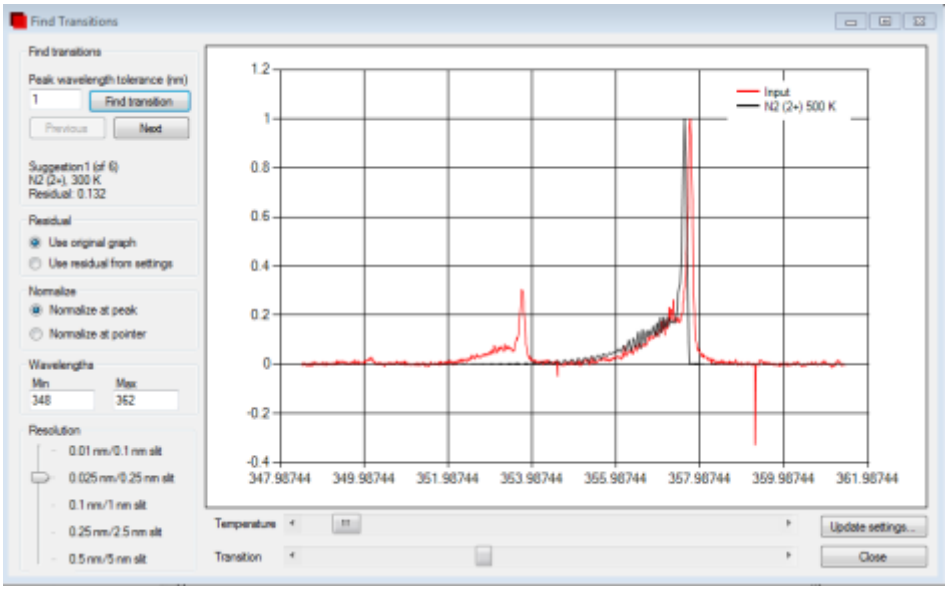

Figure 34: Window to find transitions present in the measured spectrum showing the identified transition and measured spectrum.

It is also necessary to select the appropriate resolution for the system that was used to collect the spectrum to achieve the most accurate fit as possible by using the slider shown in the bottom left of Figure 34. To identify transitions, simply click the “Find transition” button. The spectrum will look as it does in Figure 34 with the measured input spectrum in red and the identified transition in black. Next, click “Update settings” to conduct the initial calculation of the synthetic spectrum. The window shown in Figure 35 will pop up asking for initial parameters to generate the spectrum.

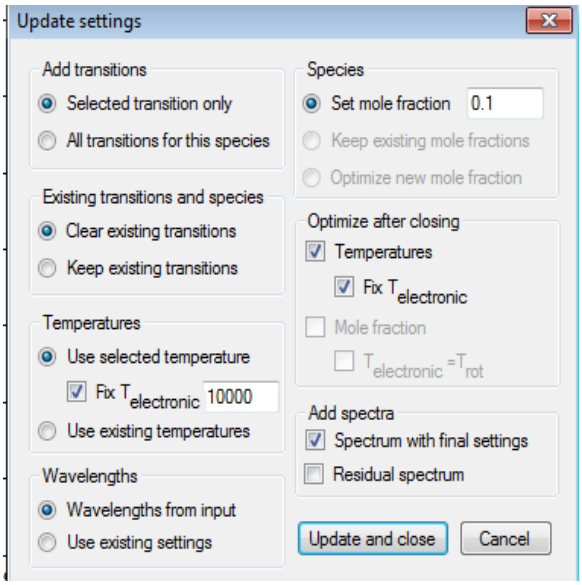

Figure 35: Initial parameters to calculate the synthetic spectrum.

As shown in figure 35 the settings should come up by default as shown except one. For non-equilibrium plasmas, the user must check the box next to "Fix $T_{electronic}$" to establish a high enough ionization to produce a transition, while this setting will not affect the temperatures calculated, it does mean that the electronic temperature is an extremely rough estimate that should not be taken as accurate. When the software finishes the initial calculations, it will display the spectra as shown in Figure A.8.

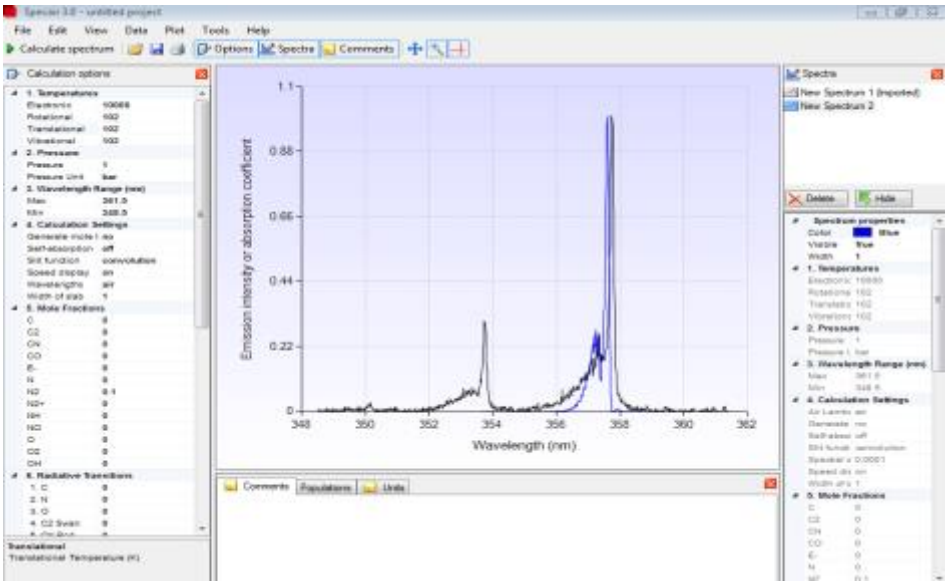

Figure 36: Initial synthetic spectrum overlaid on the imported measured spectrum.

Figure 36 shows the possibility of slight wavelength discrepancies between the measured spectrum and the fitted spectra. This can be corrected in the “Data” drop down menu at the top of the screen. One must select “Set X Values” from the options available in the “Data” dropdown menu shown in Figure 37 (a) and 37 (b).

(a)

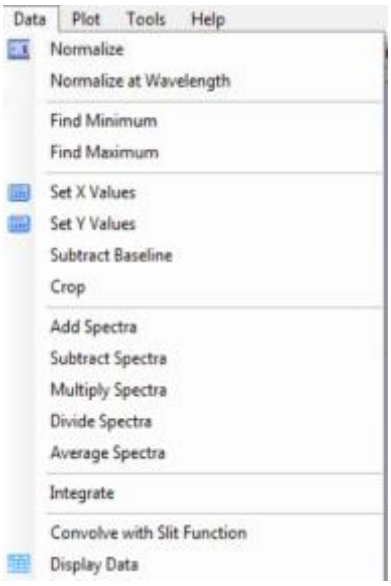

(b)

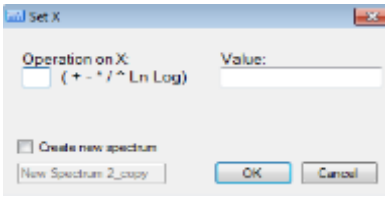

Figure 37: Data option available to correct any issues present in imported spectra.

Select the "Set X Values" as shown in Figure 37 (a) and a window shown in Figure 37 (b) will be displayed. Figure 37 (b) shows the window to correct the X values of the selected spectrum. From this window any correction needed can be made. You can add, subtract, multiply, divide, or take the natural or base 10 logarithm of the x values to make it match the accepted values. This facilitates the minimization of the residual during the fitting process to obtain the most accurate temperatures possible Once the initial synthetic spectrum matches the measured spectrum in the desired wavelength range the user can begin the final fitting process. For non-equilibrium plasma, this requires alternating between fitting the rotational and vibration temperatures while holding all other constant. Select "Fit to spectrum" from the "Tools" menu and the window presented in Figure 38 pops up.

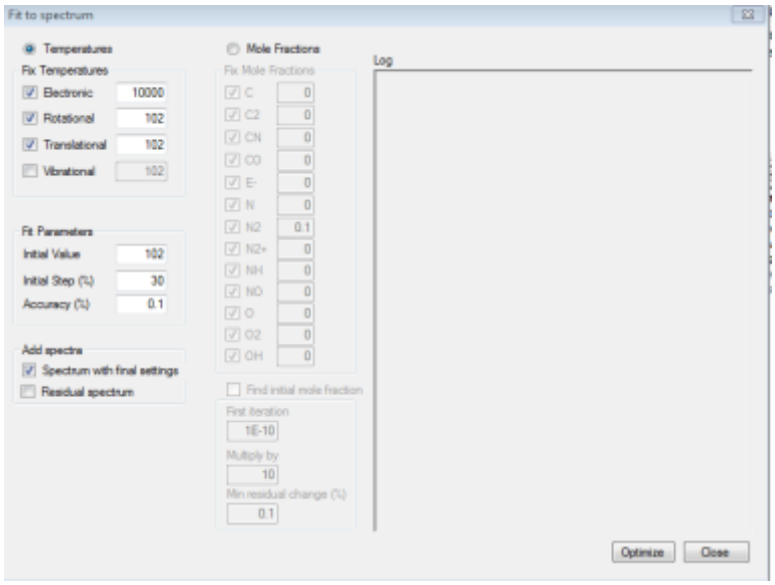

Figure 38: Fitting window that will be used to alternate fitting rotational and vibrational temperatures.

Leave the "Spectrum with final settings" box checked as this will display the new synthetic fitted spectrum on top of the initial spectra. For non-equilibrium plasmas, the only two temperatures that will matter in the fitting are the rotational and vibrational. To fit the spectra, select all the check boxes except either rotational or vibration but not both at once. The unchecked box is the temperature that will be fit. Click "optimize" and let it finish. Close the window and ensure the original imported spectrum is selected. Then repeat the process for the temperature held constant for the first fit. Alternate this procedure until an acceptable fit is achieved.

.

Appendix B

The custom MATLAB scripts were utilized to obtain normalized peak information to compare intensities of the measurements made with and without container material and bags.

```
function [ food_peaks ] = get_peak_locations( file_name,n )
%UNTITLED2 Summary of this function goes here
%   Detailed explanation goes here
x=file_name;
food_peaks=zeros(n,2);

% import data from files
IMP=importdata(x);

[pks,locs]=findpeaks(IMP(:,2));

for j=1:length(pks)
   peaks(j,1)=IMP(locs(j),1);
   peaks(j,2)=IMP(locs(j),2);
end

% Sort by second column (intensity) in descending order)
sorted=sortrows(peaks,-2);

for cont= 1:n
food_peaks(cont,1)=sorted(cont,1);
food_peaks(cont,2)=sorted(cont,2);;
end

end
```

Figure 39: Custom MATLAB scripts to obtain peaks for plotting.

VITA

VITA

Education:

Purdue University West Lafayette, IN 47907

Master of Science - Nuclear Engineering Anticipated Dec. 2016

BS Nuclear Engineering (Minor: Mechanical Engineering) May 2013
(163 undergraduate credit hours completed)

Research Experience:

Air Force Research Lab (AFRL) May. 2016 to Present
Research Engineer in DOD Pathways Program

- Developed novel diagnostics for plasma assisted ignition in SCRAMJET applications using Optical Emission Spectroscopy
- Utilized Specair software to analyze spectra obtained to resolve plasma properties
- Worked directly with senior research staff to establish and test experimental procedures pertaining to ignition experiments
- Evolved methods for spectral analysis using various experimental techniques and software packages

BioElectrics and ElectroPhysics Laboratory (BEEP) Aug. 2013 to Present
Graduate Research Assistant under Dr. Allen Garner

- Developed and implemented plasma diagnostics for plasma assisted combustion in rocket engines in collaboration with the Purdue School of Aeronautics and Astronautics
- Developed and implemented novel plasma diagnostic techniques and designed computer simulations for plasma sterilization of produce in joint project between the BEEP Laboratory and Dr. Keener of the Purdue School of Food Science
- Worked with senior faculty in Nuclear Engineering, Aerospace Engineering, and Food Science to develop and test novel technologies
- Supported and mentored three undergraduate students performing optical emission spectroscopy
- Modeling cold atmospheric pressure plasma interactions with lipid bilayers using various Molecular Dynamics codes, including LAMMPS and GROMACS

Radiation Surface Science and Engineering Laboratory (RSSEL) Aug. 2012 –May 2013
Undergraduate Research Assistant under Dr. Jean Paul Allain

- Explored material issues, including secondary electron emission in Hall thrusters and electron backscattering in ion thrusters
- Proposed multiple experiments to faculty advisor to test thruster material designs

Dr. Martín Lopez-De-Bertodano's Research Group May - Aug 2011 and 2012
Undergraduate Research Assistant/Fellow under Dr. Bertodano

- Modeled kinematic waves in vertical two phase flow regimes using Two Fluid Interfacial Temperature (TFIT) code
- Participated in Purdue's Summer Undergraduate Research Fellowship (SURF) program (Summer 2011)
  - Developed proof of concept validation of parallel computer code for linear algebra solvers related to TFIT and investigated current parallel linear algebra solvers such as ScaLAPACK and SPIKE algorithms

Teaching Experience:

Course Grader Fall 2015, Fall 2013
Grader for NUCL 305(Nuclear Instrumentation Laboratory II)

- Graded lab reports for NUCL 305 course and coordinated grading criteria with head grader to ensure consistency. Held office hours every week to assist undergraduate students

Teaching Assistant Spring 2016, Spring 2015, Spring 2014
Graduate Teaching Assistant for NUCL 205 (Nuclear Instrumentation Laboratory I) and 504 (Graduate Nuclear Instrumentation Laboratory)

- Instructed lab course two to three times a week and organized course materials and lab space. Held office hours every week to assist graduate and undergraduate students

Teaching Assistant Fall 2014
Graduate Teaching Assistant for NUCL 305 (Nuclear Instrumentation Laboratory II)

- Taught NUCL 305 lab course two to three times a week and organized course materials and lab space. Held office hours every week to assist undergraduate students

Professional Experience and Certifications:

Fundamentals of Engineering Exam (FE) April 2013

- Passed on April 13, 2013
- Indiana State Engineering Intern License #: ET31300396

A. Finkl & Sons Co. Steel Forging, Chicago, IL June – Aug. 2010

General Intern

- Organized various inventory and personnel data into different computer programs
- Communicated insurance and Workers Compensation claims to appropriate entities

Oral Presentations: ***Presenter in Italics***

R. S. Brayfield II, A. Jassem, M. Lauria, A. Fairbanks, K. Keener, and *A. L. Garner*, "Optical emission spectroscopy of high voltage, cold atmospheric pressure plasmas" 2016 IEEE International Conference on Plasma Sciences, June 2016, Banff, Alberta, Canada.

R. S. Brayfield II, "Implementation and Validation of Parallel Direct Solvers for Linear Algebraic Equations Related to Nuclear Systems Simulation" Presentation and Proceedings Paper at Summer Undergraduate Research Fellowship (SURF) Symposium, West Lafayette, IN, August 2011

Poster Presentations: ***Presenter in Italics***

A. Jassem, M. Lauria, **R. S. Brayfield II**, K. M. Keener, and A. L. Garner, "Optical emission spectroscopy diagnostics of high voltage cold atmospheric plasmas for food sterilization," The Summer Undergraduate Research Fellowship (SURF) Symposium, 06 August 2015, West Lafayette, IN (2014).

R. Brayfield II, H. M. Aktulga, A. Y. Grama, and **A. Garner**, "Molecular dynamics simulation of plasma reactive species with lipid bilayers," BioEM 2015, 16 June 2015, Asilomar Conference Center, Pacific Grove, CA, 17 June 2015, p. 91 (2015).

A. L. Garner, S. P. M. Bane, A. J. Fairbanks, B. S. Chen, **R. S. Brayfield II**, "Using electrode geometry and electric pulse parameters to control atmospheric pressure plasma formation," 2015 IEEE International Pulsed Power Conference, 01 June 2015, Austin, TX (2015).

R. S. Brayfield II, H. M. Aktulga, A. Y. Grama, and A. L. Garner, "Molecular dynamics simulations for assessing plasma reactive species interactions with lipid bilayers," 11th International Bioelectrics Symposium, October 2014, Columbia, MO, p. 25 (2014).

R. S. Brayfield II, P. Oroskar, K. Hinkle, S. Murad, A. Y. Grama, and A. L. Garner, "Molecular Dynamics Simulations of Cold Atmospheric Plasma Interactions with Lipid Bilayers," 2014 IEEE International Conference on Plasma Sciences/BEAMS, May 2014, Washington, DC.

Awards and Honors:

Best Poster (Second place) - BIOEM2015 Conference in Asilomar California June 2015

- Awarded for the annual Bioelectromagnetics Society meeting based off of judging conducted during poster sessions by senior society members

Student Travel Award - BIOEM2015 Conference in Asilomar California June 2015

- Awarded a travel grant for the annual Bioelectromagnetics Society meeting based off abstract selection for paper session

Purdue University Teaching Academy Graduate Teaching Award May 2015

- Recognized for commendable dedication to students and the material taught for the Undergraduate curriculum

Professional Organizations:

IEEE Nuclear and Plasma Science Society 2014-2015
Student Member

American Nuclear Society Student Affiliate 2010-2013
Sub-Committee chair 2012

- Oversaw efforts of assembling Glasstone award materials and completion of the application

General Member 2010, 2011, and 2013

- Directed Nuke Week activities and clean up
- Presented Nuclear Engineering related lessons to high school students

Leadership Activities:

Merrillville Community Planetarium Aug. 2004 – Present
Programmer, Volunteer

- Prepared video and sound effects in various formats for use in shows
- Updated and maintained computer networks used for computing and show presentation

Purdue Space Day 2009, 2012
Crew Member/Activity Head, Volunteer

- Designed and implemented activity in a Starlab to teach children about stars and planets
- Trained group of eight volunteers to assist in Space Day activities
- Supervised volunteers during event and assisted with Starlab presentations

Relevant Skills:

- Plasma diagnostics using optical emission and absorption spectroscopy using ICCD and CCD spectroscopy equipment
- High speed imaging
- ICCD imaging
- High voltage safety training
- Purdue Radiation Training (open/sealed sources and emergency response)
- Molecular dynamics modeling experience using LAMMPS, GROMACS, and PuReMD
- Modeled various parts and assemblies using CATIA workbenches

.

PUBLICATIONS

PUBLICATIONS

Oral Presentations: ***Presenter in Italics***

R. S. Brayfield II, A. Jassem, M. Lauria, A. Fairbanks, K. Keener, and *A. L. Garner*, "Optical emission spectroscopy of high voltage, cold atmospheric pressure plasmas" 2016 IEEE International Conference on Plasma Sciences, June 2016, Banff, Alberta, Canada.

R. S. Brayfield II, "Implementation and Validation of Parallel Direct Solvers for Linear Algebraic Equations Related to Nuclear Systems Simulation" Presentation and Proceedings Paper at Summer Undergraduate Research Fellowship (SURF) Symposium, West Lafayette, IN, August 2011

Poster Presentations: ***Presenter in Italics***

A. Jassem, M. Lauria, **R. S. Brayfield II**, K. M. Keener, and A. L. Garner, "Optical emission spectroscopy diagnostics of high voltage cold atmospheric plasmas for food sterilization," The Summer Undergraduate Research Fellowship (SURF) Symposium, 06 August 2015, West Lafayette, IN (2015).

R. Brayfield II, H. M. Aktulga, A. Y. Grama, and **A. Garner**, "Molecular dynamics simulation of plasma reactive species with lipid bilayers," BioEM 2015, 16 June 2015, Asilomar Conference Center, Pacific Grove, CA, 17 June 2015, p. 91 (2015).

A. L. Garner, S. P. M. Bane, A. J. Fairbanks, B. –S. Chen, **R. S. Brayfield II**, "Using electrode geometry and electric pulse parameters to control atmospheric pressure plasma formation," 2015 IEEE International Pulsed Power Conference, 01 June 2015, Austin, TX (2015).

R. S. Brayfield II, H. M. Aktulga, A. Y. Grama, and A. L. Garner, "Molecular dynamics simulations for assessing plasma reactive species interactions with lipid bilayers," 11th International Bioelectrics Symposium, October 2014, Columbia, MO, p. 25 (2014).

R. S. Brayfield II, P. Oroskar, K. Hinkle, S. Murad, A. Y. Grama, and A. L. Garner, "Molecular Dynamics Simulations of Cold Atmospheric Plasma Interactions with Lipid Bilayers," 2014 IEEE International Conference on Plasma Sciences/BEAMS, May 2014, Washington, DC.